International Journal of Earth Sciences (2021) 110:2435–2463
https://doi.org/10.1007/s00531-021-01992-3

ORIGINAL PAPER

Early Mississippian precollisional, peri-Gondwanan volcanic arc in NE-Mexico: Aserradero Rhyolite from Ciudad Victoria, Tamaulipas

Juan Alonso Ramírez-Fernández[1,3] · Eduardo Alejandro Alemán-Gallardo[1] · Denisse Cruz-Castillo[1] · Fernando Velasco-Tapia[1] · Uwe Jenchen[1,3] · Raúl Becchio[2,3] · Lorena De León-Barragán[1] · Juan Moisés Casas-Peña[1]

Received: 10 July 2020 / Accepted: 15 January 2021 / Published online: 13 February 2021

Abstract

The study of the pre-Mesozoic geological history of NE Mexico offers the opportunity to reconstruct the processes that occurred at the NW margin of Gondwana. The Huizachal–Peregrina Anticlinorium, which is located west of Ciudad Victoria (Tamaulipas) is a regional structure produced during the Cretaceous–Palaeogene Laramide Orogeny. Its eroded core exposes Precambrian and Palaeozoic units that together comprise the Sierra Madre Oriental basement. These units are the Neoproterozoic metamorphic Novillo Complex, the Ordovician Peregrina Tonalite, the metamorphic Pennsylvanian Granjeno Complex, and the sedimentary Silurian–Permian Tamatán Group. Aserradero Rhyolite belongs to the Tamatán Group, occurring between the siliciclastic deposits of the Early Mississippian Vicente Guerrero and the Pennsylvanian Del Monte Formations. The studied rhyolites display geochemical characteristics corresponding to high-K, low-Sr, and S-type granitoid rocks that may have been produced by upper-crustal anatexis from a source similar to that of the Novillo Complex. New LA-ICP-MS U–Pb geochronological analysis on zircons separated from the Aserradero Rhyolite yielded Early to Middle Mississippian crystallisation ages of 347.8 ± 2.7 Ma and 340.7 ± 3.6 Ma, confirming that this acidic unit is in its original stratigraphic position despite the pervasive deformation of the Tamatán Group. Based on the correlation with other Carboniferous–Early Permian magmatic complexes in Mexico and Central America, it is suggested that the Aserradero Rhyolite represents an early stage of a precollisional Carboniferous–Permian peri-Gondwanan arc, occurring also in the Las Delicias, Oaxaquia, the Acatlán Complex, the Maya Block, as well as in the buried crystalline basement along the Western Gulf of Mexico. The assembly of the Precambrian and Palaeozoic basement units from the Huizachal–Peregrina Anticlinorium were integrated with the Ciudad Victoria Block, which was dismembered from Oaxaquia and their peripheral units during the Upper-Jurassic Gulf of Mexico opening.

Keywords Carboniferous–Permian arc · Aserradero Rhyolite · Continental arc · Ciudad Victoria Block

Introduction

The Huizachal–Peregrina Anticlinorium (HPA) is a major deformation structure located west of Ciudad Victoria, Tamaulipas, that developed during the Cretaceous–Palaeogene Laramide Orogeny. Its eroded core provides a unique window into the Precambrian and Palaeozoic basement of the Sierra Madre Oriental fold-and-thrust belt in NE Mexico. Geological, geochemical, geochronological, and palaeontological studies performed during recent years have shown that this sector of the Mexican basement originated in the peri-Gondwanan realm (e.g. Ortega-Gutiérrez et al. 1995; Stewart et al. 1999; Keppie 2004; Murphy et al. 2004; Barboza-Gudiño et al. 2011; Alemán-Gallardo et al. 2019a, b).

The basement exposed in the core of the HPA includes two Palaeozoic non-metamorphosed acidic magmatic units: (a) the recently described Ordovician Peregrina Tonalite (Alemán-Gallardo et al. 2019a), which was emplaced into the Meso- to Neoproterozoic Novillo Complex, and (b) the Carboniferous Aserradero Rhyolite, included in the Palaeozoic Tamatán Group, which has been interpreted as an exotic volcanic lithodeme (Gursky and Ramírez-Ramírez

✉ Juan Alonso Ramírez-Fernández
juan.ramirezfn@uanl.edu.mx; alonso_fct@hotmail.com

[1] Universidad Autónoma de Nuevo León, Facultad de Ciencias de La Tierra, Linares, México

[2] La.Te. Andes S.A.-CONICET, Salta, Argentina

[3] Geonetwork of Latin-American German Alumni, Lima, Peru

1986; Stewart et al. 1999; De León-Barragán and Ramírez-Fernández 2012).

Although the Aserradero Rhyolite has been previously studied, its geochemical characteristics, precise age and geotectonic affinity are completely unknown. Additionally, there is no model to explain this volcanic event which occurred during the deposition of the Carboniferous marine siliciclastic units of the Tamatán group. Considering this, the main aim of the present study is to propose a geodynamic and regional palaeogeographic setting for the Aserradero Rhyolite, supported by new geochemical data and U–Pb zircon crystallisation ages.

Geological setting

Exposures of Precambrian and Palaeozoic rocks are rare in NE Mexico (Figs. 1, 2a). They are mostly covered by the Mesozoic terrestrial-to-marine sedimentary rocks of the Sierra Madre Oriental, which is an up to 3500-m-thick succession that has been described as a fold-and-thrust belt developed during the Cretaceous to Eocene Laramide Orogeny. This mountain range is part of the Mexican Orogen (Zhou et al. 2006; Fitz-Díaz et al. 2018). The HPA is a major structure of the Sierra Madre Oriental. Its eroded core contains the most complete and best-preserved outcrops of the pre-Mesozoic basement of NE Mexico. Minor basement exposures in this region are the Aramberri (Nuevo León), Miquihuana, and Bustamante (Tamaulipas) uplifted blocks (e.g., Barboza-Gudiño et al. 2011), as well as the Las Delicias area (Coahuila) (Lopez 1997; McKee et al. 1999).

The best-preserved basement outcrops of the core of the HPA are located along the canyon creeks that cut perpendicular to its major NNW–SSE-oriented fold axis. They are, from north to south: The Caballeros, Peregrina, and Novillo canyons. It is possible to recognise the exposure of four NW–SE-aligned major elements (Fig. 2b), which together comprise the above-mentioned basement. These elements include the following:

(a) The Precambrian granulitic Novillo Complex divided into a meta-igneous and a metasedimentary sector (Ramírez-Ramírez 1992; Cameron et al. 2004; Weber et al. 2010; Trainor et al. 2011; Casas-García 2014; Alemán-Gallardo et al. 2019b). This complex was previously described as Novillo Gneiss (Fries and Rincón-Orta 1965) or Novillo Metamorphic Complex (Alemán-Gallardo et al. 2019b). The Novillo Complex underwent high-grade metamorphism during the Zapotecan Orogeny, which is associated with the assembly of Rodinia (990–970 Ma; Lawlor et al. 1999; Solari et al. 2004; Cameron et al. 2004; Schulze-Schreiber 2011), with peak metamorphic conditions of 780 °C and 8.9–9.7 kbar (Orozco-Esquivel 1990). The Novillo Complex is considered the northernmost exposure of the Oaxaquia microcontinent (Ortega-Gutiérrez et al. 1995), representing the older crustal core of Mexico (Figs. 2a, b, 3).

(b) The Ordovician *Peregrina Tonalite*, a large, sheared plagiogranite pluton (Figs. 2b and 3) with subsidiary non-sheared dykes that intruded into the Novillo Complex (De León-Barragán and Ramírez-Fernández,

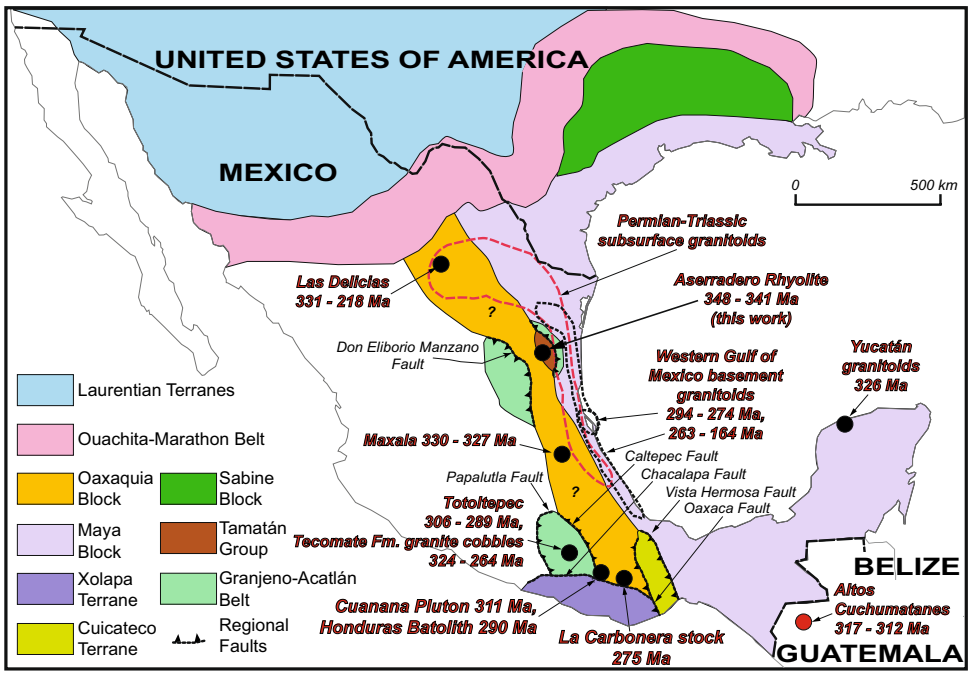

Fig. 1 Geological sketch map of Mexico and the southern United States modified after Zhao et al. (2020), following Centeno-García (2009), showing the locations of different Palaeozoic acidic igneous localities (indicated by black dots). For references of the age data see text. The major faults are drawn after Elías-Herrera et al. (2005), except Don Eliborio Manzano Fault which is proposed in this work

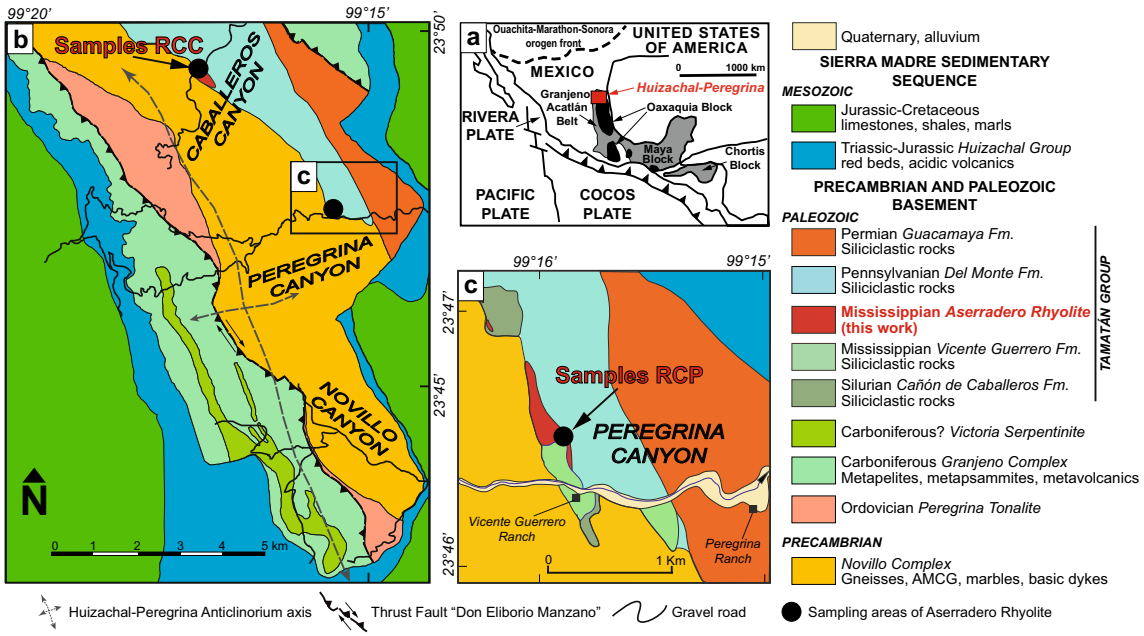

Fig. 2 **a** Sketch of the distribution of the pre-Mesozoic basement of Mexico, modified after Weber et al. (2019). The red box indicates the area of panel b. **b** Simplified geological map of the core of the southern Huizachal–Peregrina Anticlinorium, modified after Castillo-Rodríguez (1988), Ramírez-Ramírez (1992) and Alemán-Gallardo et al. (2019a). **c** Simplified geological map of Peregrina Canyon. Both figures b and c modified after Stewart et al. (1999)

2012). Fries and Rincón-Orta (1965) reported a K/Ar age of 310 ± 10 Ma for muscovites from this unit, which probably correlates with the metamorphic event of the Carboniferous Granjeno Complex. Dowe et al. (2005) reported a $^{40}Ar/^{39}Ar$ muscovite cooling age of 313 ± 7 Ma for this unit. Trainor (2010) related these Carboniferous cooling ages to the tectonic emplacement of the Granjeno Complex (see description below) against the Novillo Complex and the Peregrina Tonalite. Recently, Alemán-Gallardo et al. (2019a) reported a U–Pb zircon crystallization age by LA-ICP-MS of 448.8 ± 2.9 Ma that corresponds to the time of intrusion of the tonalite during the Late Ordovician. Similar Ordovician granites also occur in the southern Maya Block (Chiapas State in Mexico, Western Guatemala, and Belize) and are interpreted to be the northernmost extension of the South American Famatinian arc (see e.g., Ortega-Obregón 2008; Solari et al. 2010b; Estrada-Carmona et al. 2012; González-Guzmán et al. 2016; Weber et al. 2018).

(c) The Carboniferous Granjeno Complex, a lithodeme (Figs. 2b and 3) composed of a volcano-sedimentary sequence metamorphosed under greenschist-facies conditions (Carrillo-Bravo 1961; Torres-Sánchez et al. 2016), including tectonically emplaced massive and irregular serpentinitic bodies (Ramírez-Fernández and Jenchen 2016; Torres-Sánchez et al. 2017). Because this lithodeme is not composed only of schists sensu stricto, we prefer the term Granjeno Complex instead of Granjeno Schist. Dowe et al. (2005) recognised evidence of four deformational events in this complex and determined an $^{40}Ar/^{39}Ar$ cooling age of 300 ± 4 Ma (for phengite in quartz keratophyre). According to Keppie (2004) and Barboza-Gudiño et al. (2011), the deposition of the protoliths of these rocks occurred within an accretionary prism, which was located on the active margin of NW Gondwana before the Carboniferous metamorphic event. The serpentinites have been interpreted as slices of the oceanic lithospheric mantle, which accompanied the emplacement of the accretionary prism to the Precambrian continental crust (Torres et al. 2017). The contacts of the Granjeno Complex with the other basement units in the HPA's eroded core are clearly tectonic. In this context, the main fault that puts the Granjeno Complex in contact with the Novillo Complex, including the Ordovician Peregrina Tonalite and the Tamatán Group (see description below) is termed 'Don Eliborio Manzano Thrust' (Figs. 2b, 3). This fault might correlate to the Permian Caltepec fault zone, which places the Acatlán and the Oaxacan complexes of southern Mexico in tectonic contact (e.g., Elías-Herrera and Ortega-Gutiérrez et al. 2002; Elías-Herrera et al. 2005). Furthermore, a direct geological link between the Granjeno Complex and the Acatlán Complex located in southern Mexico is possible because of similarities in age, lithology,

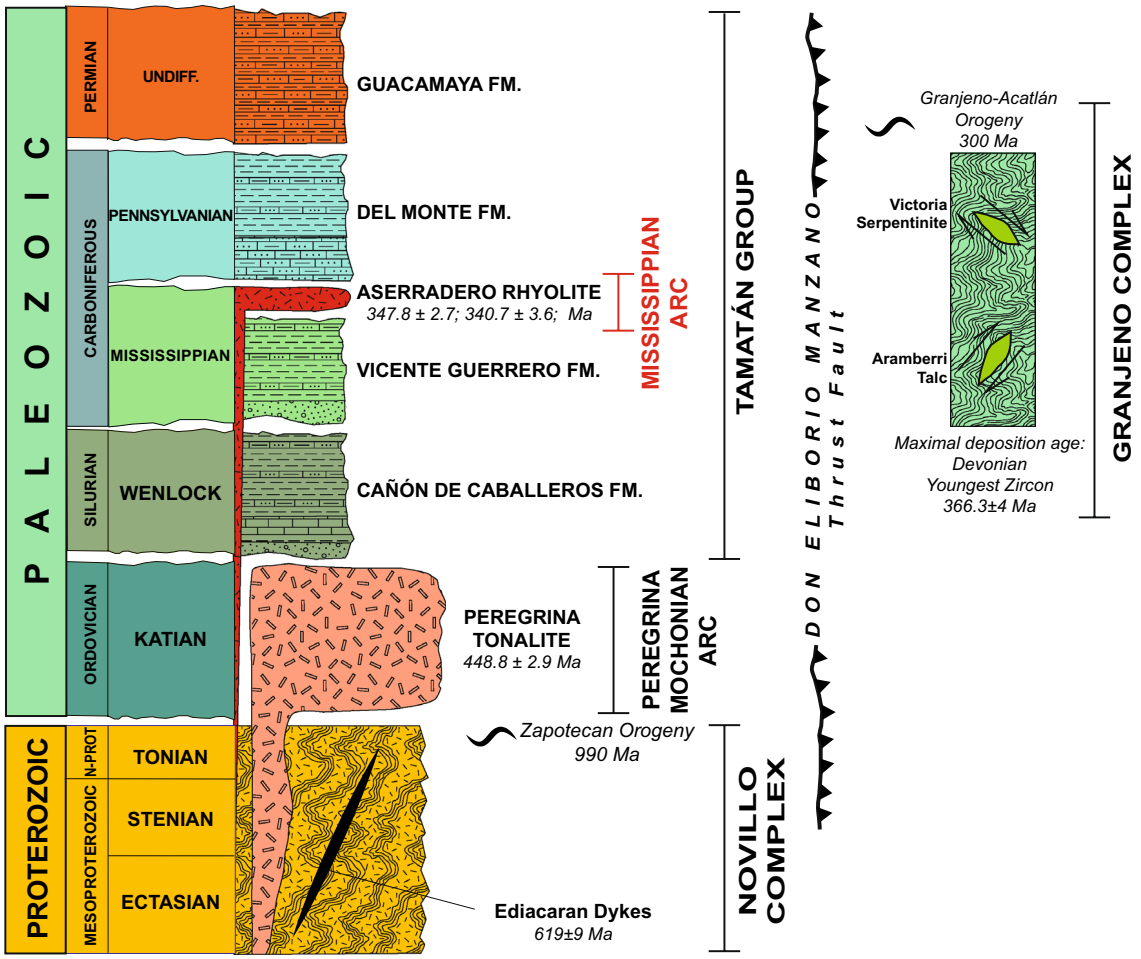

Fig. 3 Proposed stratigraphic column for the pre-Mesozoic basement in the core of the Huizachal–Peregrina Anticlinorium. With data from: Cameron et al. (2004) for the Novillo Complex; Weber et al. (2019) for the Ediacaran dykes; Alemán-Gallardo et al. (2019a) for the Peregrina Tonalite; Barboza-Gudiño et al. (2011), Dowe et al. (2005), and Torres-Sánchez et al. (2016) for the Granjeno Complex; Gursky (1996), Stewart et al. (1999), and Alemán-Gallardo et al. (2019a) for the Tamatán Group

and metamorphic grade, and together they comprise the Granjeno–Acatlán Orogenic Belt (Barboza-Gudiño et al. 2011; Torres-Sánchez et al. 2016).

(d) The Tamatán Group is a discontinuous, ca. 1650 m thick Silurian to Permian sedimentary sequence, discordantly deposited above the Novillo Complex (Gursky and Michalzik 1989). It is strongly deformed but not metamorphosed. This group comprises Palaeozoic siliciclastic and calcareous rocks (Boucot et al. 1997; Stewart et al. 1999) deposited probably in a retroarc basin bordering the NW margin of Gondwana (Alemán-Gallardo et al. 2019a; Catuneau 2004). According to Stewart et al. (1999) this Palaeozoic sequence consists of the following formations (Figs. 2b, c, 3): (a) Cañón de Caballeros (Silurian), (b) Vicente Guerrero (Early Mississippian), (c) Del Monte (Early to Middle Pennsylvanian) and (d) Guacamaya (Early Permian).

Along the Caballeros and Peregrina canyons, a ca. 80 m thick rhyolitic unit is exposed in irregular lenticular bodies, intercalated between the Mississippian Vicente Guerrero and the Pennsylvanian Del Monte Formations (Fig. 2b, c, 3). Carrillo-Bravo (1961) first described these rhyolitic bodies as Devonian novaculites (marine radiolarite) of the La Yerba Formation. However, Gursky and Ramírez-Ramírez (1986) and Ramírez-Ramírez (1992) defined these rocks as rhyolites/rhyodacites and coined the informal name '*Aserradero Rhyolite*', discarding the name 'La Yerba Formation'. Stewart et al. (1999) proposed the area of Rancho el Aserradero (23° 48.1′ W, long 99° 17.5′ N) for its type locality. The U–Pb isotope dilution-thermal ionization mass spectrometry (ID-TIMS) analyses of zircon reported by these authors yielded concordia intercept ages at 334 ± 39 Ma and 1086 ± 86, the former corresponding to the magmatic age and the latter to inheritance from the basement.

Regional Correlations

For a better understanding of the geotectonic configuration under which the Aserradero Rhyolite was generated and erupted, it is necessary to make regional correlations with other Paleozoic units from Mexico, Central America and the NW margin of South America. Currently, these are located at great distances from each other, but at the time of their development they were located closer to each other. There are no exposures of contemporaneous rocks in the vicinity of the Ciudad Victoria area.

Silurian sedimentary successions are very restricted in Mexico, in contrast to Carboniferous–Permian units (Fig. 4). Nevertheless, Silurian unmetamorphosed rocks have been documented in Venezuela. The El Horno Formation consisting of comparable lithologies (conglomerates, sandstones, siltstones, sandstones, and carbonates; Gutiérrez-Marco et al. 2011) and fauna of the Gondwanan realm (Gómez 2014), is correlative with the Silurian Cañón de Caballeros (Stewart et al. 1999). A Devonian stratigraphic gap in all records from N and SE Mexico is well-documented (Fig. 4). Nevertheless, the Bladen Formation in the Maya Mountains of Belize includes an Early Devonian volcano-sedimentary unit dated at ca. 406 Ma (Martens et al. 2010). The very low-grade metamorphosed Floresta Formation in Colombia containing Silurian or Devonian protoliths (mudstones and black shales), was re-interpreted as Carboniferous in age based on its fossil content (Cardona et al. 2016).

Carboniferous to Permian successions correlative to the Tamatán Group crop out in southern Mexico (Fig. 4). In the southernmost part of Oaxaquia, Palaeozoic sedimentary formations unconformably overlie the Oaxacan

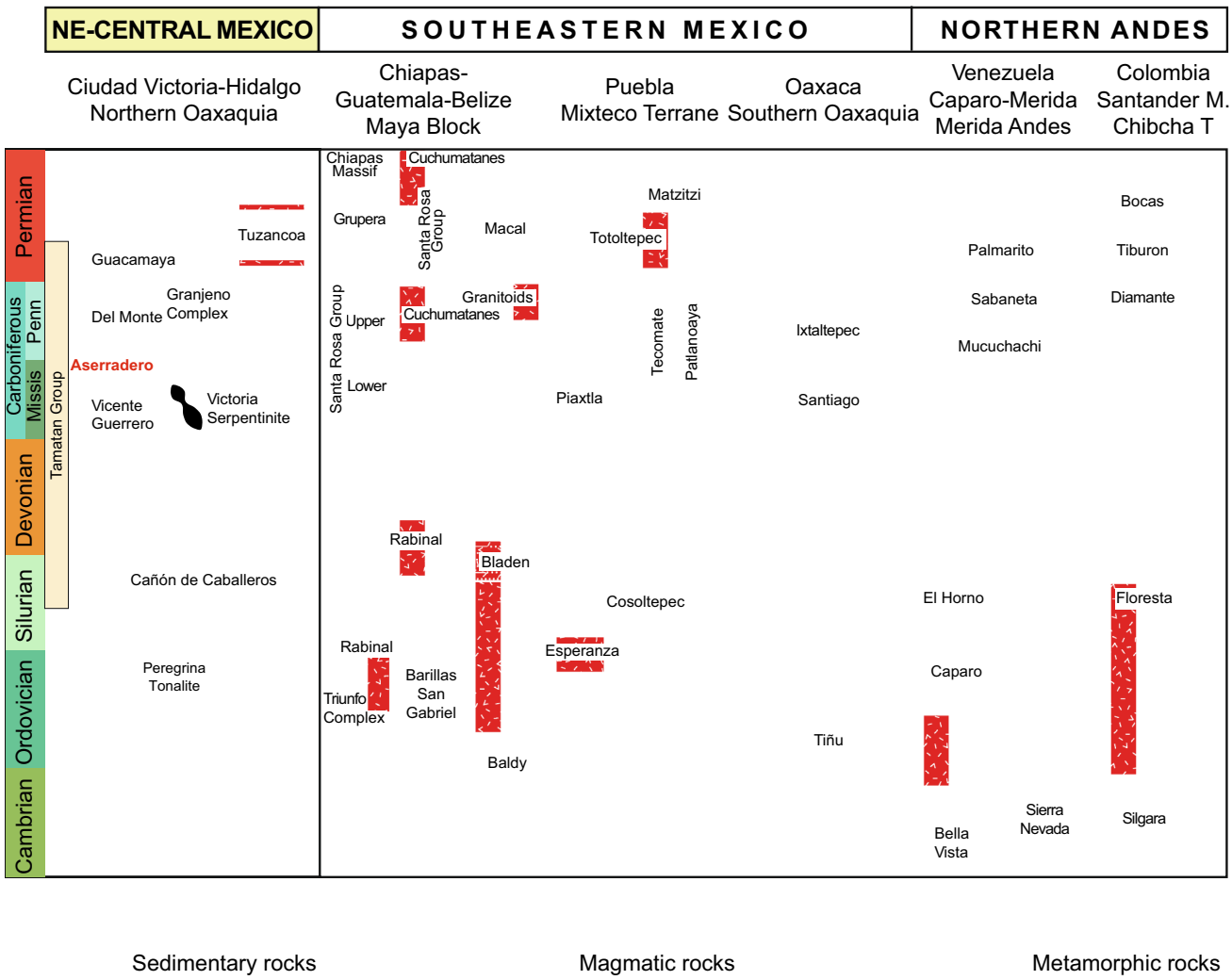

Fig. 4 Simplified Palaeozoic stratigraphy of the peri-Gondwanan terranes in Mexico and N Andes. Data are from: Stewart et al. (1999) and Alemán-Gallardo (2019b) for Ciudad Victoria and Hidalgo; Weber et al. (2009) and Martens et al. (2010) for Chiapas–Guatemala–Belize; Nance et al. (2006) for Puebla; Gillis et al. (2005) for Oaxaca; Van der Lelij et al. (2016) and Tazzo-Rangel et al. (2018) for N Andes

complex (Gillis et al. 2005) and include: (1) the Santiago Formation, consisting of limestones, shales, and minor sandstones with abundant Early Mississippian fauna (e.g., Navarro-Santillán et al. 2002). This unit correlates with the Vicente Guerrero Formation based on the similar fauna of both formations, in spite of the different lithologies (Sour-Tovar et al. 2005); (2) The Ixtaltepec Formation, consisting of shales with interbedded limestones and sandstones, and with abundant Early-Middle Pennsylvanian fauna (e.g. Flores de Dios-Gonzalez et al. 1998; Torres-Martínez and Sour-Tovar 2016), deposited in a turbiditic environment as the Pennsylvanian Del Monte Formation; (3) The Matzitzi Formation, a Permian siliciclastic succession associated with fluvial environments with abundant interbedded igneous rocks (Centeno-García et al. 2009), which is relatively younger and contrasts to the deep-turbiditic environment of the Guacamaya Formation (Stewart et al. 1999). In the Mixteco terrane of southern Mexico and adjacent to the Oaxacan complex, Late Palaeozoic sedimentary rocks unconformably overlie the Acatlán complex (e.g., Sánchez-Zavala et al. 2004). There, the Tecomate (Latest Pennsylvanian–Early Permian) and Patlanoya Formations (Early Permian) consist of siliciclastic and volcano-siliciclastic successions, which according to their fossil content (e.g., Keppie et al. 2004; Esquivel-Macías et al. 2004), can also be correlated with the Del Monte Formation (Esquivel-Macías et al. 2004). In the Maya Block (SE Mexico), the Macal unit (Belize; Martens et al. 2010) and the Santa Rosa Formation (Chiapas and Guatemala; Weber et al. 2006; 2009), consist of siliciclastic rocks and minor carbonates with sparse fossils that include species of well-established Pennsylvanian to middle Permian ages. Some authors (e.g. Rosales-Lagarde et al. 2005; Weber et al. 2006) correlate the Late Palaeozoic flysch-type sedimentary rocks with those from other terranes, for example, the northernmost part of Oaxaquia including the Las Delicias (McKee et al. 1999) and Tuzancoa Formations (Hidalgo state; Rosales-Lagarde et al. 2005) as well as the Del Monte and Guacamaya. Additionally, in northern South America, the Late Carboniferous Sabaneta and the Permian Palmarito Formations crop out (Merida, Venezuela; Laya and Tucker 2012) as well as the Diamante, Tiburón and Bocas Formations (Santander Massif, Colombia; van Der Lelij et al. 2016). Both localities include continental sandstones and conglomerates (Laya and Tucker 2012) that are contemporaneous with the Late Palaeozoic sequences of Mexico. The palaeontological record of these formations indicates that the lower part of this group evolved close to the NW Gondwana margin (near the Merida-Andes terrane, Venezuela; Stewart et al. 1999) during the Early Palaeozoic. The Tamatán Basin was located closer to Laurentia during the Late Palaeozoic, suggested by the presence of Laurentian fauna (Boucot et al. 1997; Stewart et al. 1999).

Considering these correlations, it is possible to infer that the Paleozoic units briefly described here, including those of the Tamatán Group, have shared a common peri-Gondwanan sedimentary provenance. These units most likely drifted away to their present position during the subsequent break-up of Pangea.

During the past two decades, more Carboniferous to Permian magmatic arc units have been reported in Mexico and Central America. Different interpretations and models suggest that the Carboniferous–Permian magmatic arc of Mexico and Central America is either related to the eastward subduction of the Palaeo-Pacific plate under Gondwana or to the diachronic closure of the Rheic Ocean that culminated with the assemblage of Pangaea. For this study, previously published data of Carboniferous to Early Permian acidic units from the abovementioned localities are compared with the Aserradero Rhyolite (Fig. 1). They are, from north to south:

(a) The Middle Mississippian to middle Permian (331–270 Ma) arc-related granites, rhyolites and dacites and Latest Permian to Triassic (247–215 Ma) Cordilleran calc-alkaline granodiorites, diorites, tonalites and granites from the Las Delicias area (Coahuila Terrane; Lopez 1997). The Late Palaeozoic arc rocks have been related to Alleghanian tectonism, while the Triassic plutons are the product of post-orogenic tectonics; (b) The early Permian to Middle Jurassic plutonic rocks drilled along the western margin of the Gulf of Mexico, that were interpreted to have developed in three phases (Coombs et al. 2019). The first (294–274 Ma), is represented by granitoids related to the southward subduction of the Rheic Ocean under Gondwana. During the second phase (263–243 Ma), anatectic granitoids developed under a late to post-collisional setting. During the third phase (189–164 Ma), Nazas Arc-related mafic porphyries were emplaced; (c) The Late Mississippian (326 Ma) Yucatán granitoids of the Maya Block (Zhao et al. 2020). These peri-Gondwanan adakitic granitoids were formed by crustal anatexis due to asthenospheric upwelling resulting from slab breakoff; (d) The Late Mississippian (327 Ma) Maxala Granite, belonging to the early stages of the Permian–Triassic granitoid belt in Eastern Mexico (Hidalgo and Veracruz; Martínez-Sánchez 2016) which has been associated to the subduction of the Paleo-Pacific plate; (e) The Late Pennsylvanian–early Permian (306–289 Ma) Totoltepec granitic pluton (eastern Acatlán Complex, Puebla; Kirsch et al. 2012), which has been related to the subduction of the Palaeo-Pacific oceanic lithosphere under the western margin of Pangaea; (f) The Early Pennsylvanian to Middle Permian (320–264 Ma) granitic cobbles enclosed in the Tecomate Formation of the Acatlán Complex, derived directly from the Totoletepec Pluton (Keppie et al. 2004); (g) Middle

Pennsylvanian to late Permian (311–255 Ma) felsic to mafic igneous rocks, that intruded into the Oaxacan and Acatlán complexes. According to Ortega-Obregón et al. (2014) the Cuanana pluton (ca. 311 Ma) and the Honduras batholith (290 Ma) represent the magmatic expression of the initial stages of eastward subduction of the Palaeo-Pacific plate beneath the western margin of Gondwana; (h) The early Permian (275 Ma) La Carbonera stock from the Oaxacan Complex, which appears to be part of the Permo-Triassic magmatic arc that extends from the southern United States through Mexico to Colombia (Solari et al. 2001). Its origin has been linked to the subduction of the Palaeo-Pacific plate under the western margin of Gondwana; (i) The Early Pennsylvanian granites (317 to 312 Ma, Solari et al. 2010b) from Los Altos Cuchumatanes Range in Guatemala are interpreted as the result of a E-dipping subduction zone at the convergence zone between Laurentia and Gondwana.

Considering the above review of the reported interpretations of the origin of these Carboniferous–Permian igneous rocks, the lack of a consensus regarding the dominant geotectonic process for magmatism is striking. The postulation of a comprehensive model will therefore greatly contribute to the understanding of the geological development of Mexico during the Palaeozoic before the consolidation of Pangea.

Materials and methods

Sampling

Sampling of the Aserradero Rhyolite was carried out along the creeks and slopes of the Peregrina and Caballeros canyons. Twelve samples of this unit were collected: six from Caballeros Canyon and six from Peregrina Canyon (Table 1; Fig. 2c, d). All samples were analysed by optical microscopy and used for the determination of major and trace elements as well (Table 1). Zircon crystals from two samples were separated for in situ LA-ICP-MS U–Pb dating: samples RCCD02 (Caballeros Canyon) and RCPD01 (Peregrina Canyon) (Table 2).

Preparation and analytical methods

The twelve samples selected for geochemical analyses were crushed and then pulverised in an agate bowl to obtain a fine 400-mesh powder. The analytical processes were performed at Bureau Veritas Commodities, Ltd. (Vancouver, Canada) using the LF202 package and are summarised in Table 1. Major elements were measured using inductively coupled plasma atomic emission spectrometry (ICP-AES), and trace element contents were determined using inductively coupled plasma mass spectrometry (ICP-MS). Details on these methods and their analytical precision and detection limits are available on the Bureau Veritas webpage (https://www.bureauveritas.com/um). Major oxide compositions were normalised to 100 wt% on a volatile-free basis, whereas FeO/Fe_2O_3 ratios were estimated according to the recommendations of Middlemost (1989) and using the SINCLAS software (Verma et al. 2002).

Preparation of samples RCCD02 and RCPD01 for U–Pb geochronology was performed in two parts. First, ~ 10 kg of the sampled rock was crushed and sieved at Facultad de Ciencias de la Tierra, Universidad Autónoma of Nuevo León, Mexico. Second, using conventional separation methods (sieving, magnetic susceptibility, and heavy liquids), 31 and 30 zircon crystals were separated from samples RCPD-01 and RCCD-02, respectively, and were mounted on epoxy resin and polished to nearly half their thickness to expose their internal structures at the Centro de Geociencias, Universidad Nacional Autónoma de México (UNAM). To select the most suitable areas for analysis, avoiding inclusions, fractures, and transitions between cores and rims, a cathodoluminescence scanning electron microscope was used to examine the crystal zonation. In situ U–Pb zircon dating by (LA-ICP-MS) was performed using an excimer laser workstation (Resolution M050; Resonetics) with a 23 µm spot size. The ablated material was conveyed through He gas to a quadrupole ICP-MS (iCapQc; Thermo Scientific). For more information on the methodology and instruments used in the Isotope Studies Laboratory, Centro de Geociencias, UNAM, see Solari et al. (2010a). To account for the down-hole fractionation observed in the primary standard zircon, data reduction was performed using the Iolite 2.5 software (Paton et al. 2010, 2011), and the VizualAge data reduction scheme presented by Petrus and Kamber (2012) was employed. The primary reference material used for calibration was zircon 91,500 (Wiedenbeck et al. 1995; ID-TIMS, 1065.4 ± 0.6 Ma age), and Plešovice zircon was used as a secondary control (Slama et al. 2008; ID-TIMS, 337.13 ± 0.37 Ma age). According to Solari et al. (2010a), the U–Pb ages of these reference zircons were calculated based on isotopic ratios with a precision higher than 5%. Table 2 shows the U–Th–Pb analytical data for LA-ICP-MS spot analyses. All uncertainties were propagated by attending Iolite protocols, which yielded a 2-sigma precision level (Table 2). Data were exported from Iolite, plotted using the Isoplot 3.75 software (Ludwig 2012), and shown in concordia diagrams as well as a weighted mean age plot. No common Pb correction was applied.

Results

Local geology

Although the outcrops are scarce and the geological contacts are not visible because of the dense vegetation, the Aserradero Rhyolite appears to be in a stratigraphic position

Table 1 Major (wt% by ICP-ES) and trace element (ppm by ICP-MS) geochemistry data for the Aserradero Rhyolite samples

Sample	RCCD02*	RCCB1	RCCB3	RCCB4	RCCB7	RCCB8	RCPD01*	RCPB4	RCPB6	RCPB10	RCPB9	RCPB11
Location	Caballeros Canyon						Peregrina Canyon					
Latitude	23.801901°	23.802009°	23.802009°	23.801477°	23.800882°	23.800882°	23.774606°	23.775834°	23.776150°	23.775942°	23.775942°	23.775942°
Longitude	−99.296398°	−99.296408°	−99.296408°	−99.296220°	−99.295600°	−99.295600°	−99.265812°	−99.266276°	−99.266277°	−99.266630°	−99.266630°	−99.266630°
SiO_2	75.72	76.25	78.06	75.66	74.45	69.57	68.93	76.55	74.20	76.18	76.05	72.38
TiO_2	0.03	0.03	0.04	0.04	0.03	0.05	0.04	0.03	0.03	0.03	0.03	0.03
Al_2O_3	12.80	12.70	11.18	12.31	14.4	15.89	14.83	11.46	12.99	12.42	12.67	14.48
FeO_{tot}	0.90	1.24	1.42	0.83	0.50	1.42	0.98	1.01	1.08	0.75	0.79	0.82
MnO	0.02	0.01		0.03	0.03		0.04	0.01	0.01		0.01	0.03
MgO	0.40	0.17	0.27	0.57	0.20	0.40	0.79	0.39	0.45	0.39	0.36	0.31
CaO	0.15	0.11	0.23	2.06	0.08	0.02	2.83	1.01	0.85	0.43	0.51	0.08
Na_2O	2.02	3.57	1.57	0.77	3.52	3.24	2.30	1.74	1.45	1.93	3.10	1.79
K_2O	6.08	5.35	5.68	3.91	6.27	8.73	4.30	5.09	6.43	5.69	4.74	8.59
P_2O_5	0.04	0.02	0.02	0.03	0.03	0.03	0.03	0.02	0.02	0.02	0.02	0.03
LOI	1.70	0.30	1.30	3.6	0.3	0.30	4.70	2.40	2.20	1.90	1.40	1.2
Sum	99.86	99.75	99.77	99.81	99.81	99.65	99.77	99.71	99.71	99.74	99.68	99.74
Ba	1081	1095	936	850	1080	1211	1140	1699	1364	1459	1373	1337
Be	2		9	2	1			1	2	1	2	1
Co	0.4	0.4	0.3	0.6	0.3	0.5	0.2	0.3		0.2	0.2	0.3
Cs	2.6	0.6	1.8	2	0.8	0.6	2.3	1.7	2.7	2.1	2.2	1.2
Ga	17.3	9.2	12.2	13.7	10.1	10.2	16.7	11.8	12.1	11.8	11.7	12.3
Hf	1.9	2.1	1.6	2	2	2.2	2.1	1.6	1.8	1.5	1.6	2.2
Nb	7.8	8.1	5.7	6.8	7.5	8.1	8.8	7	7.6	6.7	6.8	7.8
Rb	100.1	64.9	92.4	80.5	83.4	99.9	97.4	79.4	101.2	79	70.4	123.9
Sn	1		2	1			1					1
Sr	102.8	86.5	56.3	69.9	62	44.4	104.8	79	79.8	67.9	104.1	55.5
Ta	0.7	0.7	0.4	0.6	0.7	0.7	0.7	0.5	0.6	0.6	0.6	0.7
Th	2.9	2.9	2.5	3.1	2.9	3.2	3.7	2.7	3.6	2.6	2.9	2.7
U	1.3	1	0.9	1	0.9	1.1	1.7	1	1	1.2	1	1.1
V			9									
W		0.8	0.7	0.7	0.5	0.9						
Zr	49.8	48.5	40.7	46.5	48.4	48	50	33.9	37.8	36.8	38.2	51
Y	16.8	12.8	12.3	12.6	13.7	11.4	17.7	10.8	14.9	12.7	12.7	14.7
La	14.6	13.4	15	16.6	15.6	19.6	17.7	18.1	17.3	18.3	17.7	13.8
Ce	27.1	25.5	28.5	33	32.2	37	33.4	32.5	31.2	33.5	33.2	28.1
Pr	3.13	2.87	3.25	3.55	3.37	4.29	3.8	3.89	3.82	3.91	3.79	3.02
Nd	10.6	9.5	11.3	12.2	11.4	15.5	13.5	14.3	14	15	13	10.8
Sm	2.2	1.8	2.37	2.5	2.07	2.7	2.75	2.56	2.65	2.8	2.51	2.25
Eu	0.49	0.32	0.78	0.63	0.38	0.59	0.77	0.71	0.78	0.76	0.69	0.3
Gd	2.19	1.62	2.21	2.18	1.86	1.91	2.75	2.16	2.7	2.45	1.91	1.96
Tb	0.38	0.29	0.4	0.37	0.35	0.33	0.45	0.34	0.43	0.4	0.33	0.34

Table 1 (continued)

Sample	RCCD02*	RCCB1	RCCB3	RCCB4	RCCB7	RCCB8	RCPD01*	RCPB4	RCPB6	RCPB10	RCPB9	RCPB11
Location	Caballeros Canyon						Peregrina Canyon					
Latitude	23.801901°	23.802009°	23.802009°	23.801477°	23.800882°	23.800882°	23.774606°	23.775834°	23.776150°	23.775942°	23.775942°	23.775942°
Longitude	−99.296398°	−99.296408°	−99.296408°	−99.296220°	−99.295600°	−99.295600°	−99.265812°	−99.266276°	−99.266277°	−99.266630°	−99.266630°	−99.266630°
Dy	2.51	1.8	2	2.1	2.29	1.62	2.78	1.9	2.52	2.24	1.96	2.44
Ho	0.51	0.42	0.41	0.43	0.5	0.4	0.61	0.37	0.5	0.44	0.36	0.46
Er	1.64	1.24	1.04	1.24	1.35	1.12	1.69	0.89	1.47	1.26	1.08	1.46
Tm	0.26	0.2	0.21	0.21	0.22	0.2	0.25	0.17	0.23	0.2	0.18	0.23
Yb	1.73	1.45	1.13	1.32	1.65	1.49	1.68	1.2	1.52	1.46	1.23	1.72
Lu	0.28	0.24	0.22	0.24	0.23	0.21	0.26	0.17	0.24	0.21	0.19	0.25
Pb	2.1	20.9	6.9	37.6	1.3	16.3	4.5	72.4	5.4	15	8.8	5.4
Ni	1.3	2.3	1.6	0.6	3.1	1.6	0.4	1.7	1.7	1.1	1.3	3.3

% weight for major elements, ppm for trace elements. LOI: Loss on ignition. Blank spaces correspond to concentrations below detection limit. *Samples analyzed by LA-ICMPS on zircons for geochronology

between the Carboniferous formations (Fig. 2b, c). The collected rhyolite samples are massive and whitish in fresh cuts, containing aphanitic to microporphyritic textures. Some samples show flow foliation and devitrification spherulitic structures. Based on our field observations, the rhyolitic flows were subaerial, lacking evidence of features related to contact with water or wet sediments. Irregular, dm-sized vitreous blocks in the massive porphyric flow might indicate either a process of auto-brecciation or two distinct volcanic events (Fig. 5a).

Petrography

The Aserradero Rhyolite displays three different textural types: (a) fluidal microlithic, (b) isotropic granular, and (c) microcrystalline. The analysed rhyolites of the first type are hypocrystalline and porphyric, and include hypidiomorphic phenocrysts of plagioclase, sanidine, quartz, and biotite (sizes ≤ 1.5 mm). They are embedded in a microcrystalline quartz-feldspathic matrix, with minute accessory zircon crystals. Chlorite, sericite, pyrite, and chalcopyrite occur as secondary minerals. The matrix shows flow banding, with spherulitic devitrified areas composed by radial aggregates of quartz and sanidine. Fluidal microlithic textures are more common in samples from Peregrina Canyon (e.g., samples RCPB4 and RCPB10) compared to those from Caballeros Canyon (e.g., samples RCCB8 and RCCD2; Fig. 5b). The second textural type is isotropic granular. The rhyolite samples of this type are quartz-feldspathic and are more common in the Caballeros (e.g., samples RCCB1, RCCB3, and RCCB7) than in the Peregrina Canyon. The third textural type, the microcrystaline rhyolite, occurs in both canyons. In these samples, devitrification features are pervasive (e.g., samples RCPD-01, CPB6, CPB9, and RCCB4; Fig. 5c).

Whole-rock geochemistry

The analysed Aserradero Rhyolite samples (Fig. 2b, c; Table 1) do not show significant differences in geochemical composition. They show high concentrations of SiO_2 (68.9–78.1 wt%) and K_2O (3.9–8.73 wt%), whereas FeO, CaO, MgO, and TiO_2 contents are low (< 1.4, < 2.8, < 0.8, and < 0.05 wt%, respectively). The Al_2O_3 content ranges from medium to low (15.9–11.2 wt%). The concentrations of Zr, Th, and U are also low (< 51, < 3.2, and < 1.3 ppm, respectively), as is the Sr content (< 105 ppm).

In the total alkali–silica diagram (Fig. 6), all analysed samples plot in the rhyolite field, in concordance with their petrographic characteristics. Harker correlation diagrams on a volatile-free basis are shown in Fig. 7a–h. In the Al_2O_3 diagram (Fig. 7a), a strong and negative linear correlation with SiO_2 can be observed. FeO remains relatively constant (< 1.4 wt%, Fig. 7b) with increasing SiO_2, precluding the

Table 2 U–Th–Pb analytical data for LA-ICPMS spot analyses on zircon grains for Aserradero Rhyolite, samples RCPD-01 (Peregrina Canyon) and RCCD-02 (Caballeros Canyon)

Analysis	U (ppm)	Th (ppm)	Th/U	Corrected isotopic ratios								Rho	Corrected ages (Ma)						Best age (Ma)	± 2 s	Disc %
				$^{207}Pb/^{206}Pb$	±2σ abs	$^{207}Pb/^{235}U$	±2σ abs	$^{206}Pb/^{238}U$	±2σ abs	$^{208}Pb/^{232}Th$	±2σ abs		$^{206}Pb/^{238}U$	±2σ	$^{207}Pb/^{235}U$	±2σ	$^{207}Pb/^{206}Pb$	±2σ			
RCPD-01_22	652.0	431.00	0.66	0.0524	0.0019	0.3890	0.0170	0.0537	0.0008	0.0162	0.0007	0.10	337.0	4.6	332.8	12.0	294.0	79.0	337.0	4.6	−1.3
RCPD-01_29	475.0	191.00	0.40	0.0537	0.0018	0.3940	0.0170	0.0537	0.0008	0.0166	0.0008	0.21	337.4	5.0	338.7	12.0	339.0	73.0	337.4	5.0	0.4
RCPD-01_21	425.0	330.00	0.78	0.0535	0.0039	0.3990	0.0370	0.0539	0.0012	0.0171	0.0010	0.43	338.4	7.3	340.0	26.0	310.0	130.0	338.4	7.3	0.5
RCPD-01_30	485.0	152.00	0.31	0.0516	0.0026	0.3950	0.0220	0.0550	0.0011	0.0179	0.0012	−0.01	345.3	6.7	342.0	16.0	300.0	110.0	345.3	6.7	−1.0
RCPD-01_28	538.0	202.00	0.38	0.0527	0.0017	0.4070	0.0210	0.0554	0.0014	0.0167	0.0008	0.69	347.4	8.4	346.0	15.0	309.0	71.0	347.4	8.4	−0.4
RCPD-01_32	1840.0	1177.00	0.64	0.0529	0.0011	0.4029	0.0140	0.0554	0.0007	0.0167	0.0006	0.32	347.5	4.4	344.6	10.0	315.0	47.0	347.5	4.4	−0.8
RCPD-01_26	688.0	251.00	0.36	0.0523	0.0016	0.4030	0.0160	0.0555	0.0009	0.0180	0.0009	−0.26	348.3	5.2	343.4	11.0	309.0	73.0	348.3	5.2	−1.4
RCPD-01_18	498.0	164.90	0.33	0.0531	0.0020	0.4040	0.0180	0.0556	0.0008	0.0171	0.0009	−0.28	348.6	5.0	344.1	13.0	310.0	86.0	348.6	5.0	−1.3
RCPD-01_01	653.0	185.90	0.28	0.0535	0.0018	0.4130	0.0180	0.0558	0.0009	0.0172	0.0008	0.28	350.2	5.5	350.8	13.0	342.0	76.0	350.2	5.5	0.2
RCPD-01_12	363.0	122.30	0.34	0.0519	0.0020	0.4050	0.0210	0.0559	0.0008	0.0163	0.0008	−0.10	350.7	5.0	345.0	15.0	276.0	92.0	350.7	5.0	−1.7
RCPD-01_02	543.0	162.50	0.30	0.0543	0.0019	0.4210	0.0190	0.0560	0.0009	0.0179	0.0009	0.44	351.1	5.3	356.0	13.0	372.0	75.0	351.1	5.3	1.4
RCPD-01_03	791.0	236.60	0.30	0.0529	0.0012	0.4130	0.0150	0.0560	0.0010	0.0177	0.0008	0.55	351.4	5.9	350.8	11.0	331.0	49.0	351.4	5.9	−0.2
RCPD-01_16	476.0	341.00	0.72	0.0523	0.0020	0.4050	0.0190	0.0561	0.0009	0.0171	0.0008	0.07	352.0	5.7	344.0	14.0	277.0	85.0	352.0	5.7	−2.3
RCPD-01_17	443.0	142.20	0.32	0.0522	0.0019	0.4080	0.0200	0.0563	0.0009	0.0174	0.0008	0.32	352.9	5.5	348.0	14.0	301.0	80.0	352.9	5.5	−1.4
RCPD-01_25	377.5	173.00	0.46	0.0553	0.0023	0.4280	0.0260	0.0564	0.0020	0.0193	0.0009	0.06	353.9	12.0	361.0	18.0	390.0	94.0	353.9	12.0	2.0
RCPD-01_09	290.5	76.10	0.26	0.0514	0.0017	0.3970	0.0180	0.0567	0.0011	0.0174	0.0011	0.34	355.6	6.4	345.0	13.0	240.0	76.0	355.6	6.4	−3.1
RCPD-01_27	341.0	115.00	0.34	0.0555	0.0020	0.4370	0.0220	0.0568	0.0011	0.0193	0.0010	0.34	356.2	6.5	369.0	15.0	433.0	76.0	356.2	6.5	3.5
RCPD-01_24	386.0	104.90	0.27	0.0692	0.0016	1.5070	0.0540	0.1571	0.0023	0.0458	0.0021	0.05	940.5	13.0	932.0	22.0	894.0	48.0	940.5	13.0	−0.9
RCPD-01_06	379.0	44.90	0.12	0.0710	0.0014	1.6030	0.0560	0.1629	0.0026	0.0562	0.0034	0.36	973.0	14.0	970.0	22.0	958.0	39.0	973.0	14.0	−0.3
RCPD-01_19	207.5	48.90	0.24	0.0700	0.0023	1.6210	0.0670	0.1670	0.0035	0.0508	0.0023	0.31	996.0	19.0	975.0	26.0	910.0	68.0	996.0	19.0	−2.2
RCPD-01_23	2005.0	99.60	0.05	0.0739	0.0009	1.7530	0.0670	0.1725	0.0043	0.0516	0.0026	0.71	1025.6	24.0	1027.0	25.0	1036.0	24.0	1025.6	24.0	0.1
RCPD-01_07	208.5	74.60	0.36	0.0735	0.0021	1.7840	0.0680	0.1757	0.0027	0.0495	0.0022	0.07	1043.1	15.0	1038.0	25.0	1015.0	57.0	1043.1	15.0	−0.5

Table 2 (continued)

Analysis	U (ppm)	Th (ppm)	Th/U	Corrected isotopic ratios								Rho	Corrected ages (Ma)						Best age (Ma)	± 2 s	Disc %
				$^{207}Pb/^{206}Pb$	±2σ abs	$^{207}Pb/^{235}U$	±2σ abs	$^{206}Pb/^{238}U$	±2σ abs	$^{208}Pb/^{232}Th$	±2σ abs		$^{206}Pb/^{238}U$	±2σ	$^{207}Pb/^{235}U$	±2σ	$^{207}Pb/^{206}Pb$	±2σ			
RCPD-01_05	872.0	424.00	0.49	0.0723	0.0012	1.7730	0.0590	0.1758	0.0036	0.0524	0.0022	0.23	1044.1	20.0	1035.0	21.0	996.0	35.0	1044.1	20.0	−0.9
RCPD-01_20	153.5	38.20	0.25	0.0742	0.0017	1.8040	0.0640	0.1770	0.0026	0.0528	0.0033	0.00	1050.4	14.0	1048.0	22.0	1047.0	44.0	1050.4	14.0	−0.2
RCPD-01_15	171.0	22.80	0.13	0.0750	0.0022	1.9070	0.0920	0.1850	0.0040	0.0594	0.0041	0.54	1094.0	22.0	1090.0	29.0	1068.0	63.0	1094.0	22.0	−0.4
RCPD-01_33	758.0	70.00	0.09	0.0740	0.0010	1.8940	0.0840	0.1859	0.0065	0.0588	0.0028	0.45	1099.0	35.0	1078.0	32.0	1033.0	30.0	1099.0	35.0	−1.9
RCPD-01_14	656.0	335.00	0.51	0.0992	0.0011	2.5370	0.1000	0.1873	0.0063	0.0546	0.0028	0.88	1106.0	35.0	1282.0	32.0	1607.0	21.0	1106.0	35.0	13.7
RCPD-01_31	878.0	36.40	0.04	0.0766	0.0014	1.9920	0.0660	0.1886	0.0041	0.0665	0.0038	0.16	1114.0	22.0	1112.0	22.0	1107.0	37.0	1114.0	22.0	−0.2
RCPD-01_11	1180.0	60.40	0.05	0.0789	0.0018	2.2580	0.1100	0.2045	0.0060	0.0616	0.0028	0.76	1200.0	31.0	1199.0	33.0	1168.0	42.0	1200.0	31.0	−0.1
RCPD-01_08	157.5	55.00	0.35	0.0837	0.0016	2.7380	0.0920	0.2361	0.0037	0.0706	0.0034	0.39	1366.0	19.0	1338.0	25.0	1286.0	35.0	1366.0	19.0	−2.1
RCPD-01_04	375.0	151.40	0.40	0.0882	0.0017	3.0300	0.1900	0.2446	0.0110	0.0787	0.0035	0.88	1411.0	59.0	1413.0	50.0	1386.0	38.0	1386.0	38.0	0.1
RCCD-02_33	1675.0	706.00	0.42	0.0524	0.0012	0.3689	0.0130	0.0509	0.0008	0.0155	0.0007	0.39	319.9	4.9	318.7	9.8	293.0	54.0	319.9	4.9	−0.4
RCCD-02_02	1510.0	248.00	0.16	0.0525	0.0018	0.3740	0.0160	0.0513	0.0008	0.0172	0.0009	0.03	322.5	5.0	322.0	12.0	310.0	77.0	322.5	5.0	−0.2
RCCD-02_03	1974.0	450.00	0.23	0.0534	0.0009	0.3910	0.0150	0.0525	0.0011	0.0166	0.0007	0.27	329.7	6.6	334.8	11.0	348.0	38.0	329.7	6.6	1.5
RCCD-02_09	938.0	200.50	0.21	0.0531	0.0012	0.3870	0.0140	0.0527	0.0008	0.0171	0.0007	0.09	331.3	4.8	331.9	10.0	334.0	48.0	331.3	4.8	0.2
RCCD-02_06	2034.0	799.00	0.39	0.0532	0.0009	0.3907	0.0130	0.0533	0.0008	0.0161	0.0007	0.33	334.4	4.9	334.7	9.6	345.0	37.0	334.4	4.9	0.1
RCCD-02_29	645.0	406.70	0.63	0.0529	0.0013	0.3917	0.0150	0.0534	0.0010	0.0154	0.0006	0.28	335.5	6.0	335.3	11.0	315.0	54.0	335.5	6.0	−0.1
RCCD-02_08	1044.0	159.10	0.15	0.0526	0.0011	0.3893	0.0140	0.0535	0.0008	0.0164	0.0008	0.33	335.7	4.6	333.6	10.0	309.0	50.0	335.7	4.6	−0.6
RCCD-02_07	1080.0	175.00	0.16	0.0526	0.0014	0.3895	0.0150	0.0537	0.0008	0.0159	0.0008	0.10	337.2	4.8	333.7	11.0	297.0	59.0	337.2	4.8	−1.0
RCCD-02_18	925.0	146.20	0.16	0.0531	0.0014	0.3943	0.0150	0.0538	0.0008	0.0166	0.0009	0.13	338.0	5.0	337.3	11.0	331.0	58.0	338.0	5.0	−0.2
RCCD-02_30	1005.0	144.20	0.14	0.0524	0.0015	0.3908	0.0140	0.0544	0.0009	0.0163	0.0008	0.08	341.3	5.4	335.9	10.0	301.0	64.0	341.3	5.4	−1.6
RCCD-02_24	827.0	183.20	0.22	0.0522	0.0012	0.3948	0.0140	0.0544	0.0009	0.0166	0.0008	0.04	341.6	5.4	337.6	10.0	295.0	50.0	341.6	5.4	−1.2
RCCD-02_10	614.0	386.10	0.63	0.0532	0.0017	0.4030	0.0170	0.0545	0.0009	0.0160	0.0007	0.19	342.2	5.6	344.3	12.0	337.0	74.0	342.2	5.6	0.6

Table 2 (continued)

Analysis	U (ppm)	Th (ppm)	Th/U	Corrected isotopic ratios								Rho	Corrected ages (Ma)						Best age (Ma)	± 2 s	Disc %
				$^{207}Pb/^{206}Pb$	±2σ abs	$^{207}Pb/^{235}U$	±2σ abs	$^{206}Pb/^{238}U$	±2σ abs	$^{208}Pb/^{232}Th$	±2σ abs		$^{206}Pb/^{238}U$	±2σ	$^{207}Pb/^{235}U$	±2σ	$^{207}Pb/^{206}Pb$	±2σ			
RCCD-02_11	2195.0	410.40	0.19	0.0534	0.0010	0.4065	0.0140	0.0547	0.0009	0.0178	0.0008	0.34	343.3	5.3	346.3	9.9	355.0	43.0	343.3	5.3	0.9
RCCD-02_34	716.0	103.50	0.14	0.0521	0.0014	0.3940	0.0160	0.0547	0.0008	0.0177	0.0009	0.05	343.3	4.9	336.6	10.0	288.0	62.0	343.3	4.9	−2.0
RCCD-02_35	848.0	120.30	0.14	0.0537	0.0012	0.4080	0.0140	0.0548	0.0008	0.0165	0.0009	0.36	343.8	4.6	348.4	10.0	356.0	51.0	343.8	4.6	1.3
RCCD-02_17	1896.0	447.00	0.24	0.0531	0.0009	0.3992	0.0130	0.0548	0.0009	0.0163	0.0007	0.13	343.8	5.5	341.7	9.5	326.0	40.0	343.8	5.5	−0.6
RCCD-02_25	863.0	127.90	0.15	0.0528	0.0013	0.4019	0.0150	0.0548	0.0008	0.0156	0.0008	−0.10	344.1	5.0	342.8	11.0	317.0	58.0	344.1	5.0	-0.4
RCCD-02_05	566.0	182.10	0.32	0.0549	0.0019	0.4200	0.0170	0.0551	0.0009	0.0163	0.0008	−0.07	345.5	5.4	355.0	12.0	387.0	77.0	345.5	5.4	2.7
RCCD-02_20	850.0	113.50	0.13	0.0524	0.0019	0.3990	0.0160	0.0552	0.0009	0.0164	0.0010	−0.24	346.1	5.7	340.5	12.0	287.0	78.0	346.1	5.7	−1.6
RCCD-02_31	712.0	142.60	0.20	0.0546	0.0024	0.4170	0.0210	0.0557	0.0012	0.0175	0.0009	0.27	349.4	7.6	353.6	15.0	386.0	90.0	349.4	7.6	1.2
RCCD-02_19	1008.0	146.90	0.15	0.0521	0.0013	0.4055	0.0150	0.0557	0.0008	0.0178	0.0008	0.08	349.5	4.9	345.3	11.0	288.0	58.0	349.5	4.9	−1.2
RCCD-02_32	90.0	66.60	0.74	0.0643	0.0049	0.4960	0.0400	0.0557	0.0013	0.0178	0.0013	0.34	349.5	7.8	406.0	27.0	780.0	170.0	349.5	7.8	13.9
RCCD-02_15	1118.0	232.00	0.21	0.0529	0.0014	0.4080	0.0170	0.0558	0.0011	0.0179	0.0009	0.43	349.8	6.5	347.1	11.0	329.0	61.0	349.8	6.5	−0.8
RCCD-02_04	522.0	119.60	0.23	0.0527	0.0017	0.4090	0.0170	0.0562	0.0009	0.0177	0.0010	0.01	352.3	5.3	347.4	13.0	300.0	75.0	352.3	5.3	−1.4
RCCD-02_16	784.0	436.00	0.56	0.0509	0.0015	0.4010	0.0180	0.0563	0.0010	0.0162	0.0007	0.35	352.9	6.0	341.7	13.0	265.0	66.0	352.9	6.0	−3.3
RCCD-02_14	719.0	200.90	0.28	0.0513	0.0015	0.4040	0.0170	0.0564	0.0008	0.0172	0.0008	0.29	353.9	5.0	343.8	12.0	243.0	65.0	353.9	5.0	−2.9
RCCD-02_23	473.0	90.10	0.19	0.0574	0.0031	0.4840	0.0770	0.0598	0.0065	0.0202	0.0022	−0.16	374.0	38.0	407.0	43.0	480.0	110.0	374.0	38.0	8.1
RCCD-02_26	202.0	51.90	0.26	0.0734	0.0020	1.7600	0.1300	0.1757	0.0100	0.0513	0.0036	0.27	1043.0	59.0	1029.0	55.0	1040.0	59.0	1043.0	59.0	−1.4
RCCD-02_27	148.7	35.05	0.24	0.0785	0.0023	2.2070	0.0950	0.2024	0.0036	0.0584	0.0031	0.55	1188.0	19.0	1184.0	31.0	1173.0	56.0	1188.0	19.0	−0.3
RCCD-02_28	64.9	64.00	0.99	0.1139	0.0030	5.2800	0.2000	0.3366	0.0067	0.0934	0.0040	0.22	1869.0	32.0	1863.0	32.0	1853.0	48.0	1853.0	48.0	−0.3

U and Th concentrations are calculated employing an external standard zircon as in Paton et al. (2010)

Two sigma uncertainties propagated according to Paton et al. (2010)

$^{207}Pb/^{206}Pb$ ratios, ages and errors are calculated according toPetrus and Kamber (2012)

Analyzed spots were 23 µm, using an analytical protocol modified from Solari et al. (2010a, b)

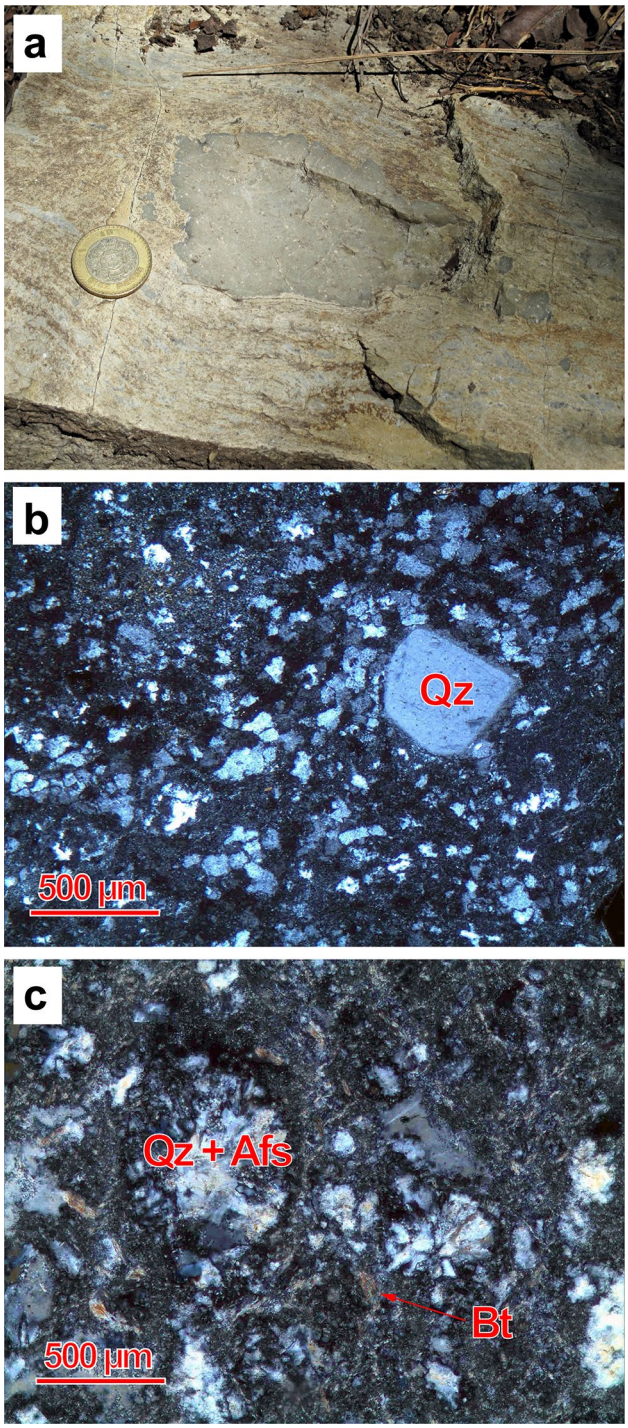

Fig. 5 **a** Volcanic flow foliation in the Aserradero Rhyolite, Caballeros Canyon. The banded rhyolite is surrounding a glassy rhyolitic fragment, probably from an older lava flow. **b** Microscopic view of sample RCCD02 (Caballeros Canyon). The texture corresponds to the fluidal microlithic type. **c** Microscopic view of sample RCPD-01 (Peregrina Canyon) with microcrystalline texture. Devitrification spherulites composed of radial quartz (Qz) and alkali feldspar (Afs) aggregates, as well as tiny, altered biotite (Bt) crystals can be observed. Images b and c taken under crossed nicols. Abbreviations after Whitney and Evans (2010)

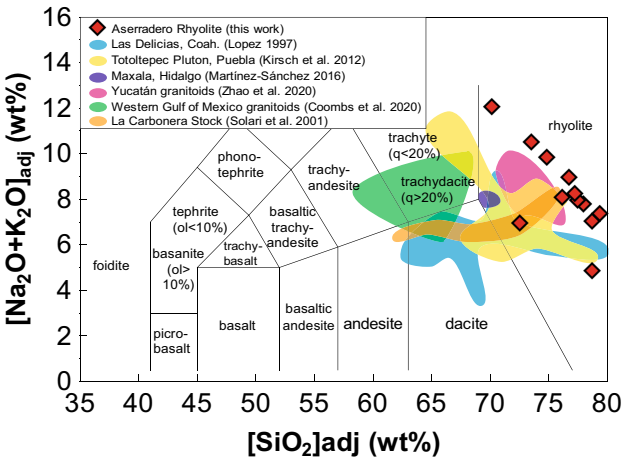

Fig. 6 Total alkali–silica classification diagram after Le Bas et al. (1986) for the Aserradero Rhyolite. Displayed for comparison are selected Palaeozoic acidic rock data from: Las Delicias, Coahuila (Lopez 1997); the Totoltepec Pluton, Puebla (Kirsch et al. 2012); Maxala (Martínez-Sánchez 2016); Yucatán granitoids (Zhao et al. 2020); Western Gulf of Mexico granitoids (Coombs et al. 2019); La Carbonera Stock (Solari et al. 2001)

fractionation of Fe-rich minerals. The studied rhyolitic samples have noticeably high K_2O concentrations (up to 9 wt %; Fig. 7c).

The Aserradero Rhyolite samples show low Zr values and relatively high Rb (Fig. 7d, e). A remarkable feature of these samples is their very low Sr and low Y concentrations (44–104 ppm, Fig. 7f, g) and low Sr/Y ratios (which remain nearly constant < 8.2, Fig. 7h).

The analysed rhyolitic unit is comparable with S-type, K_2O-rich granites, based on the K_2O vs. Na_2O plot by Chappel and White (1974) shown in Fig. 8a. According to the Frost et al. (2001) classification, the Aserradero Rhyolite samples are magnesian and show geochemical features similar to those of Cordilleran granites ([FeO/(FeO/MgO)] < 0.8) (Fig. 8b). According to the modified alkali–lime index (MALI; Frost et al. 2001), they exhibit a wide range of calcic-to-alkalic characteristics (Fig. 8c). A definition using the aluminium saturation index vs. [(Na + K)/Al] plot is not clear because the analysed rhyolites are aligned along with both the peraluminous and peralkaline fields (Fig. 8d).

The chondrite-normalised rare earth element (REE) patterns of the analysed samples are nearly parallel to each other, with a pronounced descending slope from the light REEs (LREEs) to medium REEs (MREEs) that changes to a flatter slope from the MREEs to heavy REEs (HREEs) (Fig. 9a). The $[La/Lu]_N$ ratio ranges from 5.6 to 11.4, whereas $[La/Gd]_N$ varies from 8.9 to 5.6, and $[Gd/Lu]_N$ from 1.57 to 1.00. Some samples show variable negative Eu anomalies ($\bar{x}[Eu/Eu^*]_N = 0.79$; $n = 12$), but in some cases, the patterns are nearly flat, indicating limited plagioclase

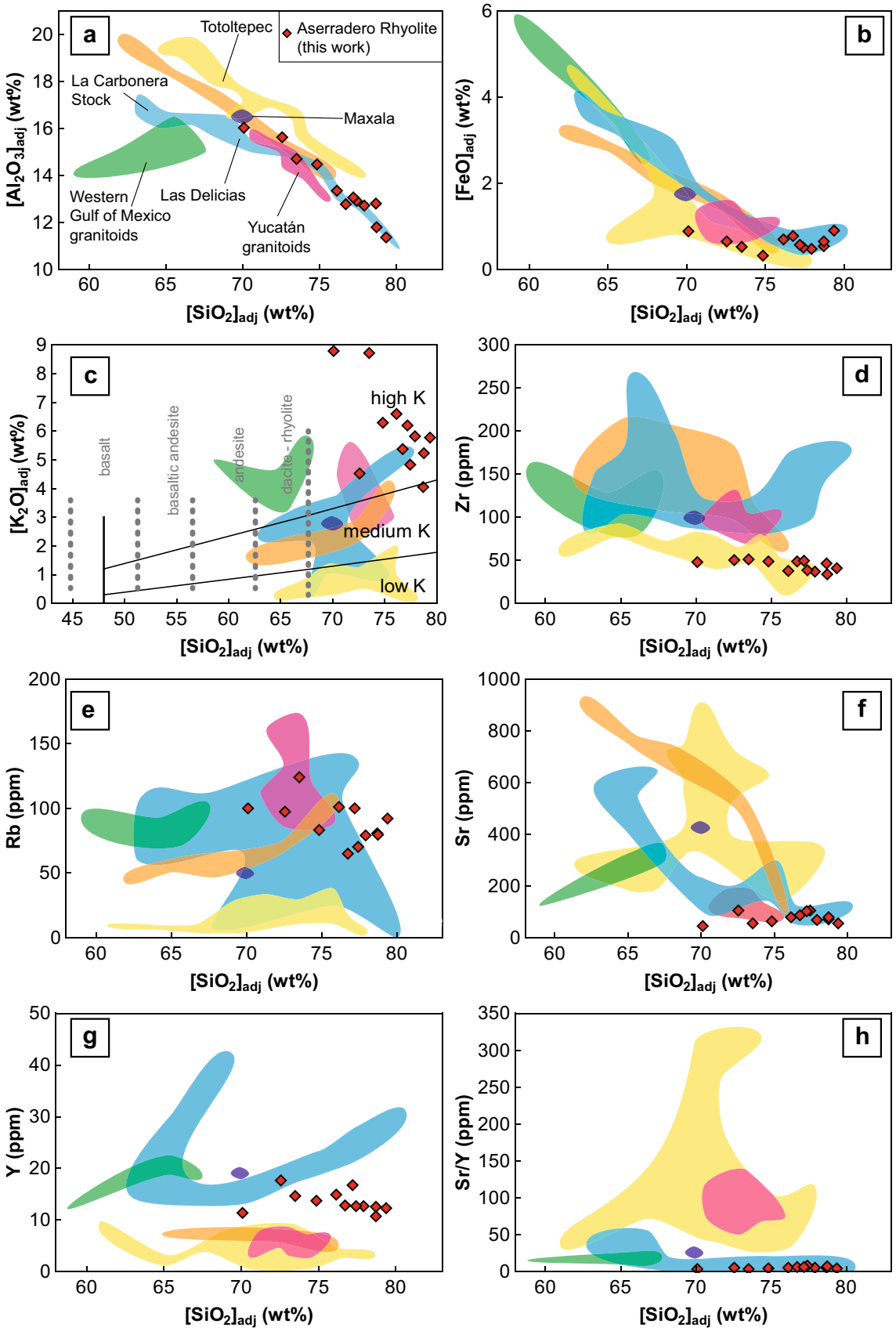
a
Totoltepec
Aserradero Rhyolite (this work)
La Carbonera Stock
Maxala
Western Gulf of Mexico granitoids
Las Delicias
Yucatán granitoids
[Al2O3]adj (wt%)
[SiO2]adj (wt%)
b
[FeO]adj (wt%)
[SiO2]adj (wt%)
c
high K
medium K
low K
basalt
basaltic andesite
andesite
dacite - rhyolite
[K2O]adj (wt%)
[SiO2]adj (wt%)
d
Zr (ppm)
[SiO2]adj (wt%)
e
Rb (ppm)
[SiO2]adj (wt%)
f
Sr (ppm)
[SiO2]adj (wt%)
g
Y (ppm)
[SiO2]adj (wt%)
h
Sr/Y (ppm)
[SiO2]adj (wt%)

◂**Fig. 7** Harker diagrams for major and trace elements and ratios for the Aserradero Rhyolite samples compared with selected Palaeozoic acidic rocks of Mexico: Las Delicias, Coahuila (Lopez 1997); the Totoltepec Pluton, Puebla (Kirsch et al. 2012); Maxala (Martínez-Sánchez 2016); Yucatán granitoids (Zhao et al. 2020); Western Gulf of Mexico granitoids (Coombs et al. 2019); La Carbonera Stock (Solari et al. 2001). **a** Al_2O_3, **b** FeO_{tot}, **c** K_2O (classification of calc-alkaline series (Peccerillo and Taylor 1976 and Le Maitre et al. 1989), **d** Zr, **e** Rb, **f** Sr, **g** Y, **h** Sr/Y. Oxides of the major elements are adjusted to a volatile-free basis

removal. The Aserradero Rhyolite samples show strong LILE enrichments and HFSE depletions compared with N-MORB. The elements Sr, P, and Ti are depleted, indicating source characteristics and fractionation processes (Fig. 9b). In contrast, the elements K and Pb are enriched in the Aserradero Rhyolite samples, which is also a feature probably inherited from the unit's source. The Cs enrichment relative to N-MORB is quite variable (85–385*x*), indicating possible alteration of the samples.

According to the Rb vs. (Y + Nb) diagram after Pearce et al. (1984) (Fig. 10a), the Aserradero Rhyolite can be interpreted as originating in a volcanic arc. In the diagram of $(Eu/Eu^*)_N$ vs. $(Gd/Yb)_N$ shown in Fig. 10b, most of the analysed samples tend to be positioned close to the compositional average of the upper continental crust (data from Lee et al. 2007).

U–Pb age and geochemistry of zircons

LA-ICP-MS U–Pb dating and trace element analyses were conducted on the 30 zircon grains separated from sample RCCD-02 (from Caballeros Canyon) and the 31 zircon grains from sample RCPD-01 (from Peregrina Canyon) (Table 2). The zircon grains show subhedral to characteristic euhedral bipyramidal habits with well-defined crystal faces.

Corrected isotope ratios and ages and their respective uncertainties are listed in Table 2, whereas trace element concentrations are shown in Table 3. Zircon isotope analysis of sample RCPD-01 yielded apparent ages ranging from 1386 ± 38 to 337 ± 4.6 Ma, with a well-defined cluster yielding a weighted mean age at 347.8 ± 2.7 Ma ($n = 17$, MSWD = 1.11; Fig. 11). The analysis of zircons from sample RCCD-02 yielded apparent ages ranging from 1853 ± 48 to 319.9 ± 4.9 Ma, with a major cluster yielding a weighted mean age of 340.7 ± 3.6 Ma ($n = 26$, MSWD = 2.8; Fig. 12). These results indicate a Mississippian crystallisation age for the Aserradero Rhyolite, corresponding to Tournaisian (Early Mississippian) and Visean (Middle Mississippian) ages for samples RCPD-01 and RCCD-02, respectively.

At least three different age populations were detected in the analysed cores of the zircon grains separated from the rhyolite (Table 2, Figs. 11, 12). These inherited zircon ages for the Peregrina Canyon sample (RCPD-01) were: (a) ~ 1.39 and ~ 1.37 Ga (Ectasian, Mesoproterozoic, $n = 2$), and (b) ~ 1.2 to ~ 0.94 Ga (Stenian–Tonian, Meso- to Neoproterozoic, $n = 12$). The Caballeros Canyon sample (RCCD-02) had two small inherited age populations: (a) ~ 1.83 Ga (Orosinian, Palaeoproterozoic, $n = 1$) and (b) ~ 1.19 and ~ 1.04 Ga (Stenian, Mesoproterozoic, $n = 2$). Most inherited zircons of both samples belong to the Stenian and Tonian periods ($n = 14$), consistent with the ages for the typically reported from Oaxaquian basement rocks (e.g., Weber and Schulze 2014).

The inherited Palaeoproterozoic, Mesoproterozoic, and Neoproterozoic cores and Carboniferous rims of the Aserradero Rhyolite zircons from both samples show geochemical parameters that contrast with each other (for example Th/U, ΣREE, $[Eu/Eu^*]_N$, and $[Gd/Lu]_N$). The Carboniferous zircon rims have Th/U ratios of 0.26–0.78 ($\bar{x} = 0.42 \pm 0.16$; sample RCPD-01) and 0.14–0.74 ($\bar{x} = 0.27 \pm 0.17$; sample RCCD-02), supporting its magmatic origin. A Th/U ratio of 0.1 is considered a general threshold between metamorphic and igneous zircon (e.g., Hoskin and Schaltegger 2003; Rubatto 2017). The '*typical Oaxaquia*' (sensu Weber and Schulze 2014) inherited cores from sample RCPD-01 (1.2 to 0.94 Ga, Stenian to Tonian) have Th/U ratios of 0.04 to 0.51, whereas the cores from sample RCCD-02 (1.19 and 1.04 Ga) show Th/U of 0.23 and 0.25, respectively. Inherited cores related to '*Proto-Oaxaquia*' (1.39 and 1.37 Ga, sensu Weber and Schulze 2014) have Th/U of 0.40 and 0.35, similar to '*typical Oaxaquia*' cores. The Palaeoproterozoic (1.85 Ga) core presents a Th/U ratio of 0.99 (sample RCDD-02), significantly higher than those of any other grain analysed here.

The sums of the REE contents of the analysed zircons are highly contrasting, depending on if they are magmatic or inherited. The Carboniferous rims of the zircons from sample RCPD-01 have ∑REE of 1767 to 4308 ppm (average: 2926 ± 687 ppm), whereas those of sample RCCD-02 display ∑REE of 1216 to 7022 ppm (average: 4441 ± 1226 ppm). The Meso- to Neoproterozoic cores have significantly lower REE concentrations. Sample RCPD-01 inherited grains have ∑REE of 268 to 1548 ppm (average: 789 ± 458 ppm), whereas those from sample RCDD-02 have ∑REE of 210 and 354 ppm. The unique Palaeoproterozoic grain from sample RCCD-02 yielded a REE sum of 382 ppm. The chondrite-normalised REE patterns (Fig. 13a, b) also suggest that all the zircons are magmatic in origin. The Carboniferous zircon rims from both samples (Fig. 13a) have negative Pr and Eu anomalies, a positive Ce anomaly, and LREE (~ 0.1 to 100*x*) to HREE (~ 1000 to 50,000*x*) enrichment. The inherited cores show similar behaviour in Fig. 13b. These patterns are typical for unaltered magmatic zircons (e.g., Hoskin and Schaltegger, 2003). Just one single Carboniferous magmatic rim shows a flat HREE-pattern, due to higher La, Pr, and Nd contents. The U/Yb vs. Hf and U/Yb vs. Nb/Yb correlation diagrams for zircons after Grimes

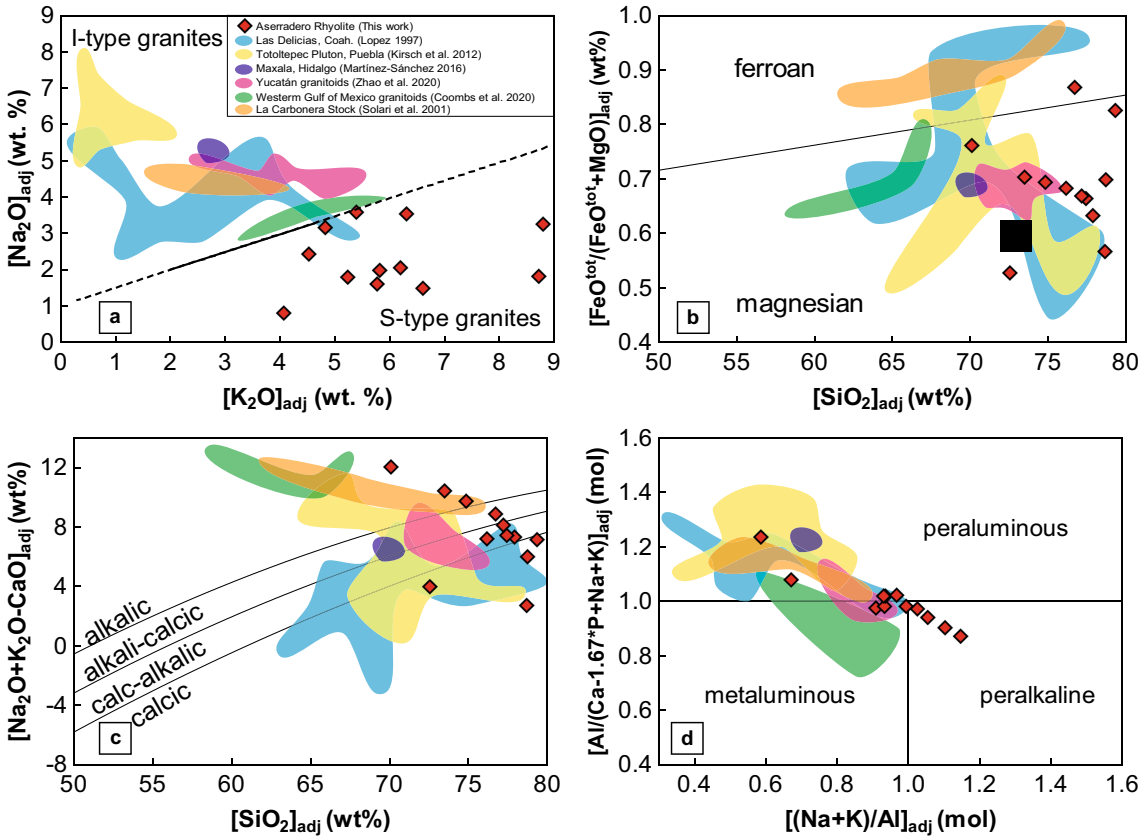

Fig. 8 Geochemical comparison of Aserradero Rhyolite samples with selected Palaeozoic acidic rocks of Mexico: Las Delicias, Coahuila (Lopez 1997); the Totoltepec Pluton, Puebla (Kirsch et al. 2012); Maxala (Martínez-Sánchez 2016); Yucatán granitoids (Zhao et al. 2020); Western Gulf of Mexico granitoids (Coombs et al. 2019); La Carbonera Stock (Solari et al. 2001). **a** Plot K_2O vs. Na_2O after Chappell and White (1974). **b** FeO/(FeO + MgO) vs. SiO_2 (wt%) diagram. **c** $Na_2O + K_2O - CaO$ vs. SiO_2 (wt%) diagram. **d** [Al/(Ca-1.67P + Na + K)] (mol) vs. [(Na + K)/Al] (mol) diagram. Diagrams 8 b–d after Frost et al. (2001). Oxides of the major elements are adjusted to a volatile-free basis

et al. (2015) are shown in Fig. 14a, b. All analysed points, cores and rims, plot in the same fields: 'crustal input' and 'magmatic arc array'. Nevertheless, the higher crustal input in the inherited cores is noticeable.

Discussion

According to the new geochemical data and precise geochronology presented here, the Aserradero Rhyolite represents an early stage of a Carboniferous-Permian continental arc along the northwestern margin of Gondwana. The study of its palaeographic position is important to understand the prevailing geodynamic conditions of this margin before the assembly of Pangaea.

Local geological implications

The subaerial flows of Aserradero Rhyolite indicate an important hiatus in the stratigraphic record of the Tamatán Group. The deposits of the underlying Early Mississippian Vicente Guerrero Formation represent shallow-marine conditions, whereas those of the overlying Pennsylvanian Del Monte Formation indicate proximal conditions, based on the presence of coarse conglomerates, sandstones, and debris flow deposits (Stewart et al. 1999). It is plausible to suggest that the subaerial eruption of the Early to Middle Mississippian Aserradero Rhyolite postdates a deformational and/or uplifting event, which affected only the underlying sedimentary units.

Whole-rock geochemistry

The Aserradero Rhyolite is the most acidic among all compared Palaeozoic samples. Despite their local emplacement mechanisms, the majority of the compared samples can be classified geochemically as rhyolites and dacites, with minor trachytes and trachyandesites (Totoltepec pluton and the western Gulf of Mexico granitoids; Fig. 6). In Harker diagrams (Fig. 7a, b) the compared Carboniferous-Early

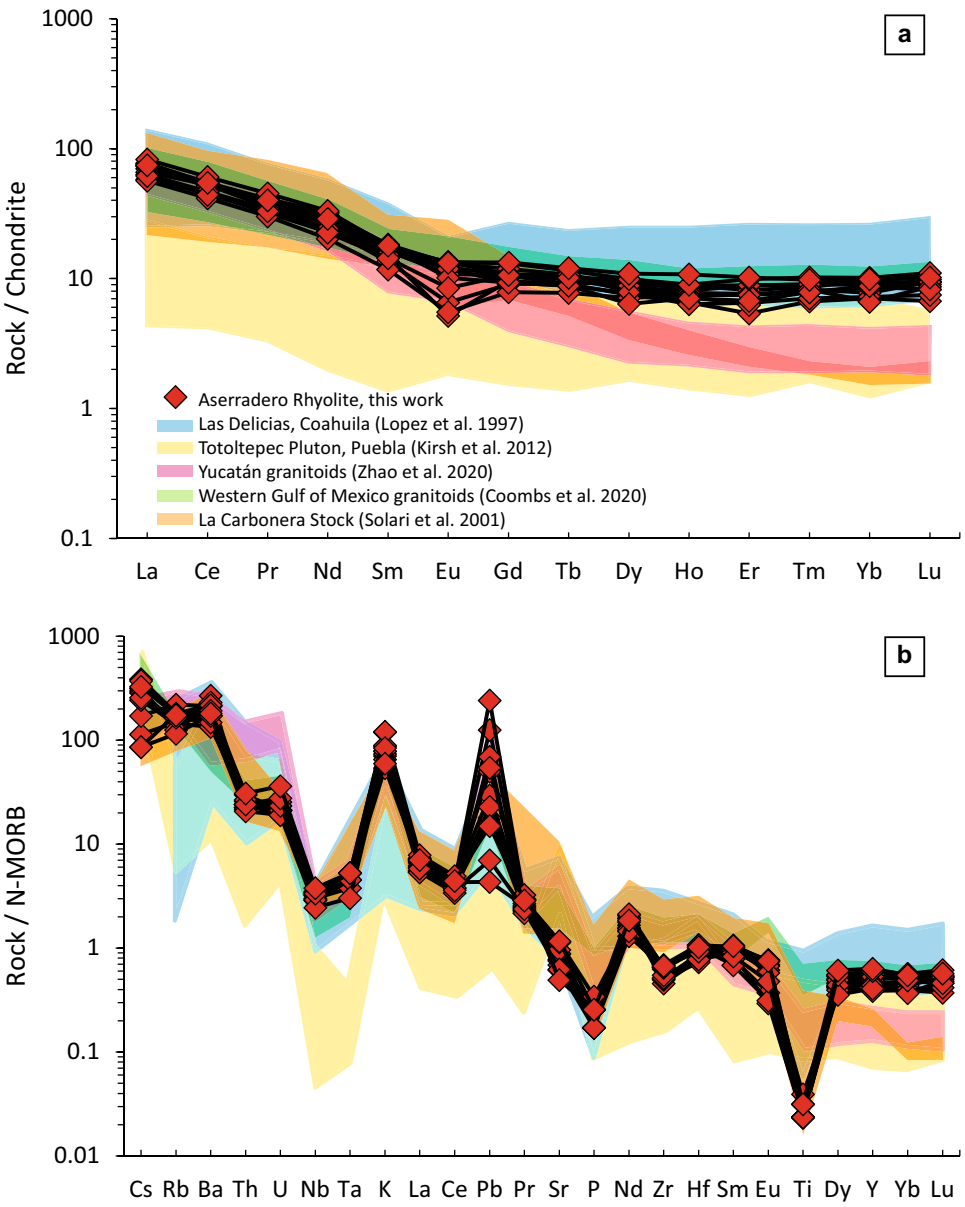

Fig. 9 Normalised trace element diagrams for the Aserradero Rhyolite and selected Palaeozoic acidic rocks of Mexico: Las Delicias, Coahuila (Lopez 1997); the Totoltepec Pluton, Puebla (Kirsch et al. 2012); Maxala (Martínez-Sánchez 2016); Yucatán granitoids (Zhao et al. 2020); Western Gulf of Mexico granitoids (Coombs et al. 2019); La Carbonera Stock (Solari et al. 2001). **a** Chondrite-normalised rare earth element (REE) diagram. **b** Multi-element diagram. Normalisation values after Sun and McDonough (1989)

Permian suites show a significant overlap in Al_2O_3 and FeO concentrations with negative linear correlations. The schemes of Peccerillo and Taylor (1976) and Le Maitre et al. (1989) show that the Aserradero Rhyolite samples as well as the western Gulf of Mexico granitoids are characterized as high-K (Fig. 7c). In contrast, the Las Delicias rocks show the highest variation in this diagram, with K_2O ranging from low to high-K, whereas the Totoltepec samples show the lowest K_2O values. The La Carbonera Stock and the Maxala samples are medium-K. The Yucatán granitoids fit into the medium-K and the lower part of the high-K fields. In the Zr, Rb, Sr and Y diagrams, all the localities show high dispersion with no clear patterns.

Aserradero Rhyolite samples display Na_2O and K_2O concentrations similar S-type granites (Fig. 8a), whereas the rest of the compared samples plot in the I-type granite field. The high-K character and low Sr and Y concentrations of the Aserradero Rhyolite are consistent with the model of generation of granitic melts by intracrustal melting of plagioclase-rich igneous protoliths, probably of tonalitic to granodioritic composition, at moderate crustal levels (e.g., Drüppel et al. 2009). Annen et al. (2006), suggesting that mantle-derived hydrous basalts from subduction zones were intruded as a succession of sills into the lower crust generating a deep crustal hot zone, where pre-existing meta-sedimentary and meta-igneous crustal rocks get melted. These silicic melts can form volcano-feeding magma chambers or shallow plutons. Ducea et al. (2015) considered higher Sr/Y ratios (> 25) to indicate a deeper crustal origin for processing magmas. Because this ratio positively correlates with

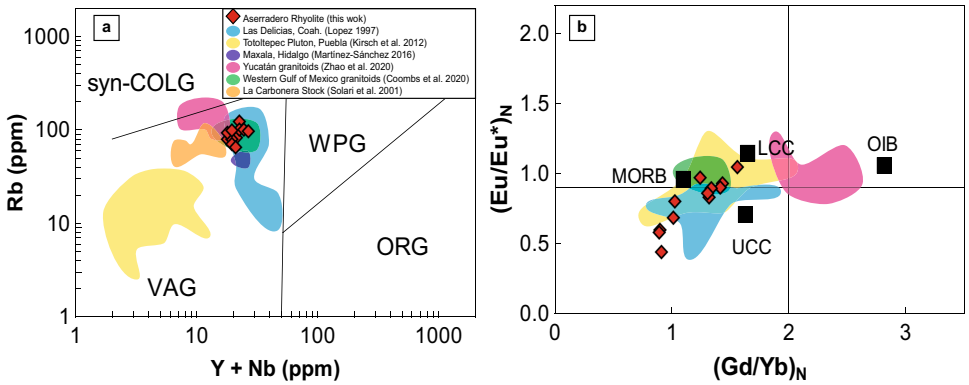

Fig. 10 Tectonic discrimination diagrams and correlation of selected trace element ratios for the Aserradero Rhyolite and compared Palaeozoic acidic magmatic rocks of Mexico: Las Delicias, Coahuila (Lopez 1997); the Totoltepec Pluton, Puebla (Kirsch et al. 2012); Maxala (Martínez-Sánchez 2016); Yucatán granitoids (Zhao et al. 2020); Western Gulf of Mexico granitoids (Coombs et al. 2019); La Carbonera Stock (Solari et al. 2001). **a** Rb vs. (Y + Nb) (ppm) diagram from Pearce et al. (1984). **b** Ta vs. Yb (ppm) diagram from Pearce et al. (1984). **c** CR-(IA + CA)-COL discrimination diagram from Verma et al. (2012). *CR* continental rift, *IA* island arc, *CA* continental arc, *COL* collisional. **d** $(Eu/Eu^*)_N$—$(Gd/Yb)_N$ geochemical variation diagram. *N-MORB* normal mid-ocean ridge basalt, *OIB* ocean island basalt, *LCC* lower continental crust, *UCC* upper continental crust

the increasing crustal thickness of modern arcs, the Aserradero Rhyolite may have originated by shallow-level anatexis, based on its very low Sr/Y ratios (3.8–8.2; Fig. 7h).

According to the FeO/(FeO + MgO) ratio (Fig. 8b) the Aserradero Rhyolite as well as almost all compared Carboniferous–Early Permian rocks have a magnesian character, except for the La Carbonera Stock and some samples from Las Delicias that are ferroan. In the modified alkali–lime index diagram (Fig. 8c) the samples from the La Carbonera Stock and the western Gulf of Mexico granitoids show an alkalic character, whereas the Las Delicias rocks and the Yucatán granitoids samples range from calcic to alkali–calcic. The Totoltepec pluton samples show a wide dispersion range as well as the Aserradero Rhyolite samples, ranging from alkalic to calcic. Most of the compared samples are dominantly peraluminous, except for some samples from the western Gulf of Mexico granitoids that fall in the metaluminous field (Fig. 8d).

The REE patterns of the Aserradero Rhyolite are similar to those of the western Gulf of Mexico granitoids and the Las Delicias rocks. The Yucatán granitoids and the La Carbonera Stock samples show the same pattern with a constant slope from LREE to HREE (Fig. 9a); by contrast, the Totoltepec samples are the least REE-enriched. In general, all samples analysed for this contribution show similar arrays in the N-MORB-normalised multi-elemental diagram (Fig. 9b). All of them display noticeable negative Nb–Ta anomalies, a typical feature detected in arc magmas (Pearce and Peate 1995). They also show negative P and Ti anomalies and high, positive K and Pb anomalies.

According to the discrimination diagram of Pearce et al. (1984) (Fig. 10a), the Aserradero Rhyolite is related to a volcanic arc tectonic setting similar to the rest of Carboniferous samples. The $(Eu/Eu^*)_N$ and $(Gd/Yb)_N$ ratios of the Aserradero Rhyolite (Fig. 10b) plot close to the average composition of the upper continental crust. According to Frost et al. (2001), magnesian high-K alkali–calcic granitic rocks occur in Cordilleran batholiths, associated with delamination of over-thickened crust. In contrast, S-type granitoids typically form by partial melting of sedimentary protoliths during thermal relaxation and/or exhumation of an orogenic system (Chappel and White 1974; Frost et al. 2001), and they are not associated with coeval mafic rock. Hence, chemical features are consistent with our interpretation that the Aserradero Rhyolite erupted during a period of crustal exhumation.

Zircon geochronology

Within errors, the age of Aserradero Rhyolite is the same as reported previously by Stewart et al. (1999). Nevertheless, the new data have a much better precision, indicating two distinct volcanic events. Now, Aserradero Rhyolite volcanism is well defined with ages that range from 347.7 ± 2.7 to 340.7 ± 3.6 Ma. These ages confirm that the stratigraphic level of the Aserradero Rhyolite fits well within the Tamatán Group, regardless of the intricate structural character of this unmetamorphosed Palaeozoic sequence (Figs. 3, 15).

Only one inherited zircon from the Cañón de Caballeros sample has a concordant Palaeoproterozoic age (~ 1.85 Ga), not yet reported from Oaxaquia (see e.g., Ortega-Gutiérrez et al. 1995; Solari et al. 2004; Weber and Schulze 2014). Weber et al. (2010) determined a similar upper-intercept age of 1.82 Ga for a single discordant grain from the Huiznopala Gneiss, which represents the oldest zircon ever measured in an Oaxaquia sample. This Palaeoproterozoic grain can

Table 3 Trace element analysis on zircon grains for rhyolite RCCD-02 from Caballeros Canyon and for rhyolite RCPD-01 from Peregrina Canyon by ICP-MS

Analysis/ppm	Ti	Y	Nb	La	Ce	Pr	Nd	Sm	Eu	Gd	Tb	Dy	Ho	Er	Yb	Lu	Hf	Pb	Th	U
RCCD-02_02	3.4	7400	22.80	0.163	10.6	0.17	2.67	9.6	2.02	85.4	41.6	584.0	261.0	1303.0	2860	558	16,390	65.25	248.0	1510
RCCD-02_03	2.7	5550	27.10	0.015	15.3	0.06	1.88	8.3	2.21	70.6	33.8	475.0	197.6	956.0	2026	400	15,890	82.25	450.0	1974
RCCD-02_04	4	3860	3.27	0.031	6.7	0.09	1.52	5.7	1.56	49.7	22.3	311.0	135.0	654.0	1520	316	14,100	27.28	119.6	522
RCCD-02_05	3.9	3930	4.76		10.7	0.04	2.00	7.1	2.26	53.1	22.8	321.0	139.7	686.0	1557	326	13,120	27.88	182.1	566
RCCD-02_06	3.1	6070	30.90		26.6	0.07	2.05	10.9	2.93	94.0	38.7	521.0	212.3	989.0	2065	412	15,680	99.25	799.0	2034
RCCD-02_07	2.7	9990	7.80	0.054	8.5	0.08	1.76	9.1	2.30	99.0	51.3	762.0	335.0	1630.0	3430	693	14,900	49.75	175.0	1080
RCCD-02_08	2.7	7700	8.62	0.011	6.7	0.04	1.00	6.3	1.79	75.9	38.5	584.0	259.0	1296.0	2860	580	16,840	52.70	159.1	1044
RCCD-02_09	1.3	7390	8.22	5.000	15.8	0.84	5.80	8.7	2.16	78.1	37.4	522.0	230.7	1157.0	2560	517	15,970	50.18	200.5	938
RCCD-02_10	7.8	4860	7.98	0.056	24.7	0.19	3.48	10.7	4.01	87.0	32.7	419.0	166.4	772.0	1626	327	13,750	30.08	386.1	614
RCCD-02_11	4.1	7440	31.20	0.167	16.7	0.22	3.26	10.0	2.52	89.4	40.5	594.0	250.0	1204.0	2640	509	18,390	106.25	410.4	2195
RCCD-02_14	2.5	5530	6.72	0.011	11.3	0.09	2.26	8.4	2.72	73.4	31.0	433.0	183.6	890.0	1896	389	14,860	36.58	200.9	719
RCCD-02_15	7.4	6890	10.19	0.520	11.1	0.23	1.90	8.3	2.65	78.1	36.7	529.0	224.0	1097.0	2470	496	15,250	54.00	232.0	1118
RCCD-02_16	6.1	5170	15.69		43.0	0.14	2.70	8.2	3.30	73.1	29.8	410.0	171.8	801.0	1698	337	11,110	36.10	436.0	784
RCCD-02_17	3.1	6350	21.88	0.034	12.1	0.08	1.48	7.6	1.64	70.7	34.1	480.0	199.1	969.0	2002	393	14,960	93.75	447.0	1896
RCCD-02_18	2.6	7200	6.22		6.5	0.04	1.18	6.9	1.77	73.3	35.6	516.0	228.2	1117.0	2490	494	15,210	44.88	146.2	925
RCCD-02_19	6.4	7480	6.81	0.051	6.6	0.06	1.25	7.1	1.87	72.9	36.3	541.0	232.9	1139.0	2574	506	14,680	47.40	146.9	1008
RCCD-02_20	3.4	7350	5.22		4.6	0.02	0.85	5.4	1.26	64.7	34.1	517.0	231.6	1160.0	2632	530	15,740	43.55	113.5	850
RCCD-02_23	0.9	3590	10.70	0.520	13.7	0.13	1.47	3.0	1.25	36.5	17.5	256.0	109.0	559.0	1430	275	13,000	23.75	90.1	473
RCCD-02_24	2.3	6000	6.17	0.043	9.1	0.07	1.85	7.7	2.40	68.9	31.5	440.0	190.0	931.0	2070	415	14,810	39.03	183.2	827
RCCD-02_25	4	7500	4.93	0.217	5.7	0.11	1.94	7.0	1.80	70.2	34.7	512.0	232.0	1151.0	2620	525	15,860	44.15	127.9	863
RCCD-02_26	4.4	324	4.97		5.5		0.59	1.9	0.37	10.9	3.1	31.3	11.2	47.1	81.9	16.5	10,630	40.08	51.9	202
RCCD-02_27	14.5	538	3.01		4.1	0.02	0.41	1.4	0.20	9.7	3.8	45.9	17.6	80.2	158.1	32.4	10,760	30.43	35.1	148.7
RCCD-02_28	18.9	535	2.54		18.2	0.07	1.45	3.0	0.51	13.5	4.3	49.8	18.1	82.8	159	30.9	10,320	20.93	64.0	64.9
RCCD-02_29	5.9	3260	11.15		29.7	0.05	1.66	5.8	2.21	44.5	18.1	243.0	102.4	498.0	1109	234	11,930	33.08	406.7	645
RCCD-02_30	1.7	8330	6.23	0.059	6.3	0.05	1.42	7.2	2.06	78.6	38.8	573.0	255.2	1253.0	2770	550	15,550	47.90	144.2	1005
RCCD-02_31	10.8	8390	16.80	0.093	14.1	0.28	4.73	17.0	4.78	118.5	48.8	631.0	249.0	1171.0	2460	481	12,540	34.00	142.6	712
RCCD-02_32	11.6	1565	2.23	0.062	7.7	0.27	3.71	6.1	3.53	32.5	10.2	123.0	48.4	239.4	606	135	7940	4.25	66.6	90
RCCD-02_33	2.8	7160	20.90	0.020	21.6	0.13	2.49	10.5	2.96	85.0	38.8	539.0	218.5	1054.0	2250	443	14,490	70.15	706.0	1675
RCCD-02_34	3.6	6290	14.60		10.4	0.03	0.76	5.0	1.38	53.6	27.5	426.0	192.0	963.0	2160	431	15,060	36.13	103.5	716
RCCD-02_35	3	8410	5.32		5.5	0.02	1.08	6.7	1.60	72.4	38.3	574.0	256.0	1282	2840	576	16,550	48.03	120.3	848
RCPD-01_01	3.6	5280	20.00		23.7	0.05	1.40	5.5	2.26	55.1	26.5	380.0	164.7	811.0	1798.0	362.0	14,300	36.68	185.9	653.0
RCPD-01_02	5.3	4780	17.11		23.8	0.04	1.54	4.7	2.18	52.8	24.7	349.0	150.4	731.0	1631.0	334.0	14,380	31.65	162.5	543.0
RCPD-01_03	4.7	6460	27.30	0.041	27.6	0.07	1.81	8.0	2.50	75.6	33.0	467.0	200.9	969.0	2099.0	423.0	15,140	46.58	236.6	791.0
RCPD-01_04	17.5	1380	3.63	0.050	34.2	0.10	2.66	4.9	1.20	28.6	9.5	112.0	46.0	221.0	530.0	116.0	10,670	99.00	151.4	375.0
RCPD-01_05	5.4	817	1.95	0.031	9.2	0.02	0.19	0.9	0.52	8.3	3.8	53.5	25.0	136.5	398.0	89.6	13,090	133.25	424.0	872.0
RCPD-01_06	11.1	1157	1.13		1.9	0.08	1.30	4.7	0.26	28.0	10.0	114.4	38.7	167.4	291.0	55.1	13,910	65.00	44.9	379.0
RCPD-01_07	3.5	397	0.41		3.8	0.00	0.19	0.6	0.17	4.2	2.0	27.0	12.1	65.2	175.3	40.0	13,110	36.83	74.6	208.5

Table 3 (continued)

Analysis/ppm	Ti	Y	Nb	La	Ce	Pr	Nd	Sm	Eu	Gd	Tb	Dy	Ho	Er	Yb	Lu	Hf	Pb	Th	U
RCPD-01_08	2.8	2200	2.53		5.4	0.21	3.96	9.4	1.62	52.4	18.2	212.0	80.3	330.0	540.0	100.0	11,230	39.43	55.0	157.5
RCPD-01_09	2.5	2460	7.66		12.4	0.04	0.63	2.9	1.21	29.1	12.2	181.0	79.7	382.0	882.0	184.0	15,140	17.25	76.1	290.5
RCPD-01_11	6.7	1410	29.90	0.031	8.2	0.08	0.41	1.4	0.14	13.2	6.7	100.0	46.7	259.0	787.0	164.0	14,640	185.00	60.4	1180.0
RCPD-01_12	2.9	3280	5.44		14.4	0.10	2.28	7.1	2.55	50.2	19.2	255.0	105.2	499.0	1088.0	214.6	13,490	19.58	122.3	363.0
RCPD-01_14	25.3	1760	8.50	0.243	26.7	0.11	2.01	4.4	0.33	27.4	11.6	149.0	58.7	282.0	564.0	107.0	14,430	143.50	335.0	656.0
RCPD-01_15	4.1	324	2.52	0.078	1.6	0.05	0.53	1.2	0.49	5.9	2.3	24.6	9.1	49.9	191.0	51.0	13,990	27.63	22.8	171.0
RCPD-01_16	5.1	5240	7.18	0.176	28.5	0.25	4.40	13.2	4.45	90.0	35.3	425.0	165.0	770.0	1570.0	313.0	12,490	27.25	341.0	476.0
RCPD-01_17	4.4	3780	7.29		15.5	0.07	1.86	5.2	2.07	49.6	20.9	280.0	118.7	569.0	1275.0	259.0	13,780	23.68	142.2	443.0
RCPD-01_18	3.7	4260	6.96		17.1	0.06	1.34	6.2	2.17	50.8	22.9	322.0	136.8	657.0	1455.0	297.0	13,520	27.40	164.9	498.0
RCPD-01_19	19.7	2060	3.16	0.068	4.6	0.10	1.86	6.1	0.56	45.6	15.2	190.0	74.2	332.0	730.0	147.5	15,730	33.48	48.9	207.5
RCPD-01_20	3.1	340	0.38	0.003	2.4		0.10	0.3	0.16	3.3	1.5	22.3	10.5	54.9	160.6	36.3	11,840	26.68	38.2	153.5
RCPD-01_21	7.7	3700	6.10	0.147	37.0	0.20	3.50	9.5	4.10	65.0	24.6	330.0	123.0	590.0	1120.0	227.0	11,020	18.75	330.0	425.0
RCPD-01_22	5.5	5530	9.06	0.047	34.6	0.23	4.42	11.2	5.16	84.1	32.4	431.0	175.0	830.0	1760.0	362.0	12,010	31.60	431.0	652.0
RCPD-01_23	19.6	610	3.73	0.259	2.5	0.29	4.03	7.7	1.72	36.9	10.3	83.0	18.4	51.5	47.0	6.8	11,840	324.50	99.6	2005.0
RCPD-01_24	6.7	454	5.84	0.000	30.2	0.10	2.18	5.3	0.20	25.2	7.2	60.0	15.6	51.7	61.4	9.0	14,390	50.33	104.9	386.0
RCPD-01_25	4.1	3690	4.80	0.077	24.3	0.16	3.11	8.8	3.59	61.1	21.6	293.0	118.2	569.0	1195.0	249.0	10,660	22.85	173.0	377.5
RCPD-01_26	5.2	3300	15.51	0.003	21.7	0.05	1.27	4.7	1.88	40.9	18.0	249.0	108.0	530.0	1211.0	240.0	12,520	30.70	251.0	688.0
RCPD-01_27	4.2	2660	5.74	0.000	12.0	0.02	0.79	3.3	1.66	33.1	14.1	197.0	82.7	409.0	936.0	192.5	13,570	18.45	115.0	341.0
RCPD-01_28	6.6	5090	17.30	0.105	27.1	0.24	3.77	11.5	4.93	78.9	32.6	409.0	159.4	738.0	1533.0	302.0	12,250	26.75	202.0	538.0
RCPD-01_29	4.2	3880	4.59		16.3	0.08	1.85	6.3	2.77	51.7	21.3	293.0	127.2	608.0	1376.0	280.0	11,880	23.75	191.0	475.0
RCPD-01_30	3.2	3490	4.21	0.003	11.6	0.01	1.08	4.5	1.69	43.0	17.8	253.0	109.0	548.0	1260.0	256.0	13,020	22.00	152.0	485.0
RCPD-01_31	6.6	1565	3.96	0.330	3.4	0.03	0.73	2.4	0.73	15.6	8.9	126.8	51.2	240.0	492.0	86.5	14,190	129.50	36.4	878.0
RCPD-01_32	7	5820	36.00		43.0	0.09	2.81	12.0	3.86	91.3	36.2	458.0	183.0	849.0	1750.0	343.0	15,020	98.50	1177.0	1840.0
RCPD-01_33	23.5	829	1.73		7.4	0.10	1.23	3.5	0.32	22.2	8.9	94.0	27.6	105.0	144.0	39.3	14,600	164.50	70.0	758.0

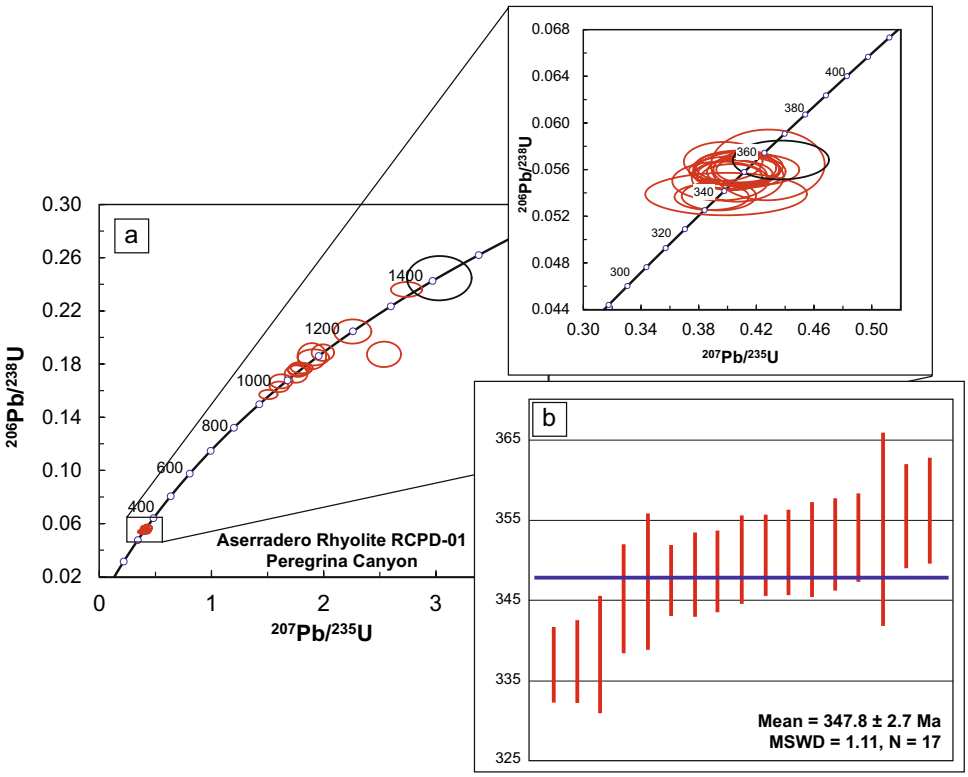

Fig. 11 U–Pb dating results of the Aserradero Rhyolite sample RCPD-01, from Peregrina Canyon. **a** Concordia plot for zircon data. Ellipses show ± 2σ uncertainty ranges. **b** Best age is the weighted average $^{206}Pb/^{238}U$ age of 347.7 ± 2.7 Ma, based on 17 analyses

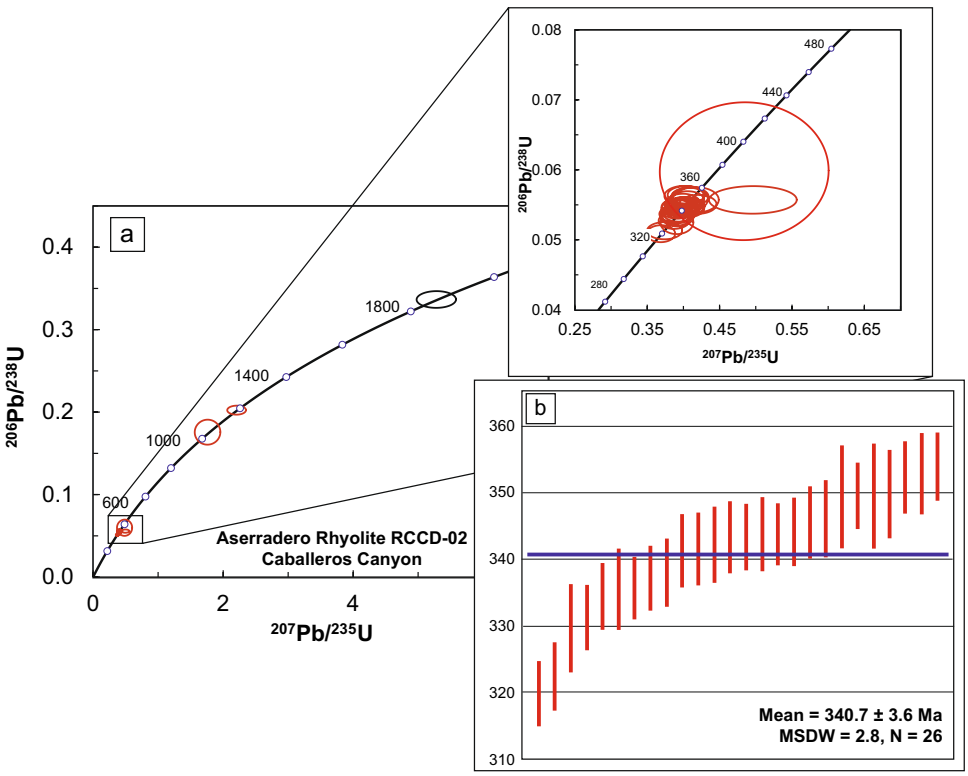

Fig. 12 U–Pb dating of the Aserradero Rhyolite sample RCCD-02, from Caballeros Canyon. **a** Concordia plot for zircon data. Ellipses show ± 2σ uncertainty ranges. **b** Best age is the weighted average $^{206}Pb/^{238}U$ age of 340.7 ± 3.6 Ma, based on 26 analyses

be derived from a cratonic source from Amazonia crustal domains, such as Rio Negro–Juruena (1.8–1.55 Ga) or Ventuari–Tapajos (1.95–1.8 Ga) (Ibañez-Mejía et al. 2018). Another possibility is that the rhyolitic magma assimilated sediments with detrital zircons from older cratonic sources.

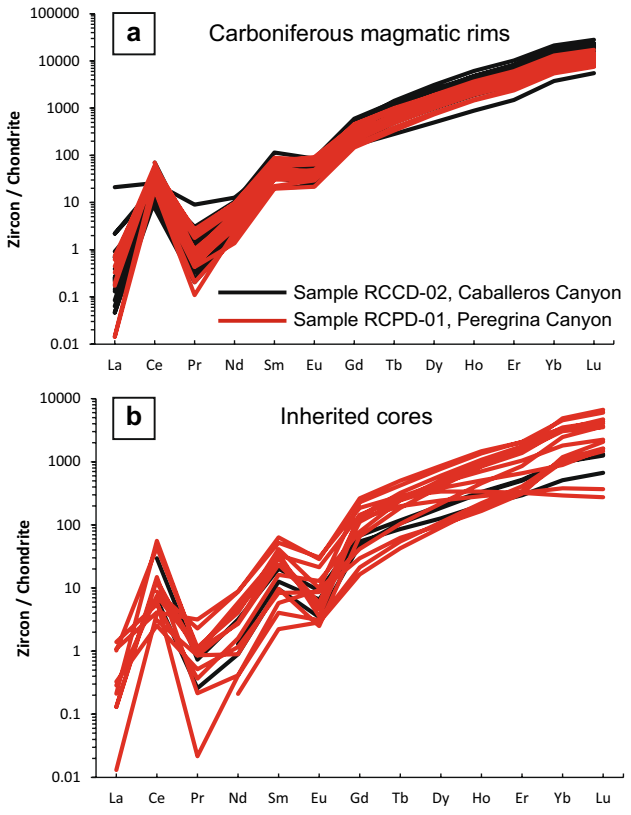

Fig. 13 Chondrite-normalised REE patterns for zircons from the Aserradero Rhyolite. **a** Carboniferous magmatic rims. **b** Inherited cores. Normalising values after McDonough and Sun (1995)

The inherited Mesoproterozoic (1.39 and 1.37 Ga) zircons from Cañón de Peregrina sample may correspond to the '*proto-Oaxaquia*' oceanic arc system, which was possibly active during the breakup of the former supercontinent Columbia (~ 1.5–1.4 Ga, age based on Lu–Hf isotopic compositions; Weber and Schulze 2014). Nonetheless, these grains can be derived from cratonic sources, like the Putumayo Orogen of northwestern South America, which originated from the collisional incorporation of Amazonia to the assembling Rodinia Supercontinent (Ibañez-Mejía et al. 2018). The first phase of this orogen comprises an arc system and craton-derived sediments deposited over the Amazonian continental margin, between 1.33 and 1.15 Ga, and perhaps as early as 1.45 Ga. On the other hand, early Mesoproterozoic zircon grains may be derived from Late Neoproterozoic to early Paleozoic sedimentary sequences like the Jocote and Baldy units of Mexico's Chiapas State and Belize, respectively, where 1.5–1.4 Ga detrital zircon grains are common (e.g., Martens et al. 2010; González-Guzmán et al. 2016).

The inherited Meso- to Neoproterozoic zircons (1200–940 Ma; Stenian-Tonian) from both samples correspond to '*typical Oaxaquia*' events (Cameron et al. 2004; Weber et al. 2010): the 'old suite' island arc (ca. 1.23–1.11 Ga), the AMCG (anorthosite–mangerite–charnockite–granite) suite, which developed after the collision of Oaxaquia against Amazonia (~ 1.03–1.01 Ga); and the Zapotecan granulite facies orogeny resulting from the later collision of Baltica (~ 990–970 Ma) with Amazonia.

As shown in the Fig. 15, the emplacement sequence of the Carboniferous–Permian magmatic arc starts with Aserradero Rhyolite, followed by the Maxala Granite (Martínez-Sánchez, 2016), the Yucatán granitoids (Zhao et al. 2020), the Totoltepec Pluton (Kirsch et al. 2012; cobbles from Tecomate Fm., Keppie et al. 2004), Altos Cuchumatanes, Guatemala (Solari et al. 2010b), the Cuanana Pluton (Ortega-Obregón et al. 2014), Las Delicias (Lopez 1997), Western Gulf of Mexico granitoids (Coombs et al. 2019), La Carbonera Stock (Solari et al. 2001) and Chiapas Massif granitic protoliths (Weber et al. 2007). From these units only the Aserradero Rhyolite, Altos Cuchumatanes, Chiapas Massif and the Totoltepec Pluton have inherited zircons, mostly related to Oaxaquia and the Maya Block.

For a better reconstruction of the geological events recorded in the Ciudad Victoria region, it is also important to consider previous geochronological determinations for the Ordovician Peregrina Tonalite. Dowe et al. (2005) reported a Middle Pennsylvanian muscovite $^{40}Ar/^{39}Ar$ cooling age of 313 ± 7 Ma, matching with the 310 ± 10 Ma K/Ar muscovite age obtained earlier by Fries and Rincón-Orta

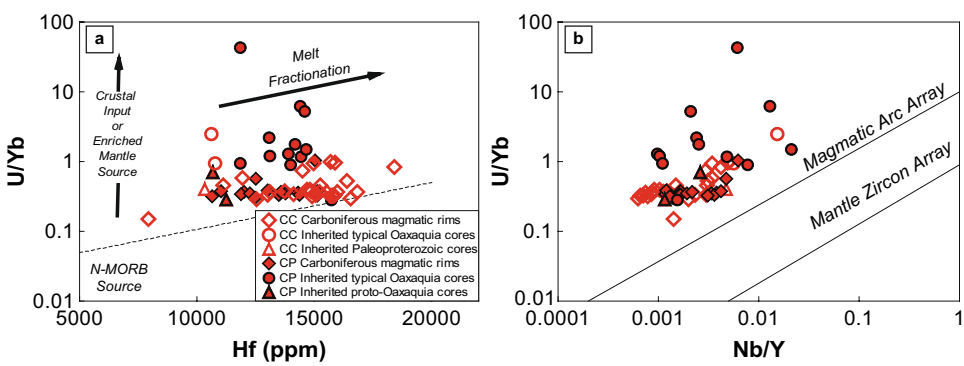

Fig. 14 U/Yb-based zircon discrimination diagrams after Grimes et al. (2015) for Precambrian inherited cores and Carboniferous magmatic rims from the Aserradero Rhyolite, samples RCPD-01 (Peregrina Canyon, PC) and RCCD-02 (Caballeros Canyon, CC). **a** U/Yb vs Hf (ppm). **b** U/Yb vs. Nb/Yb

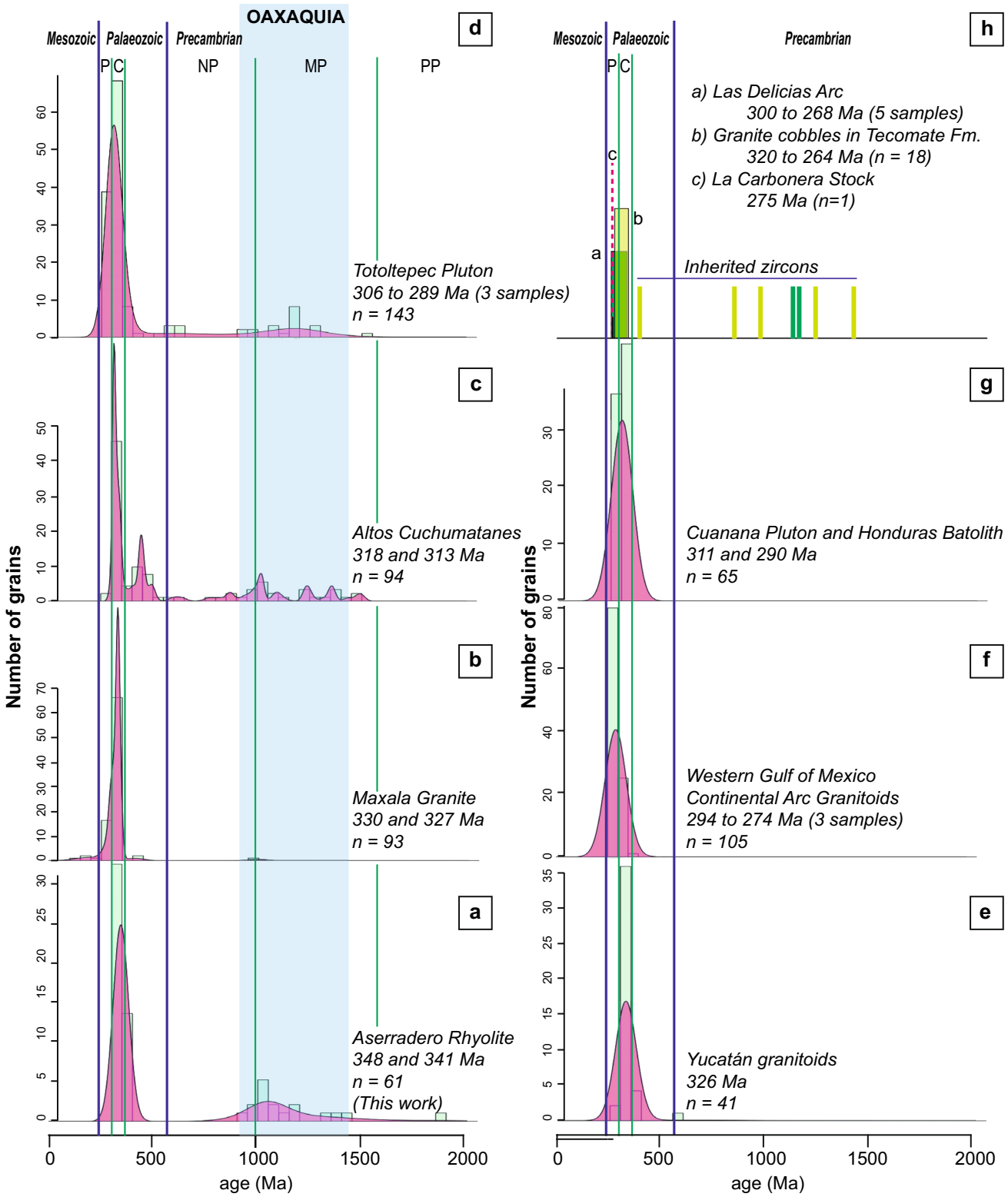

Fig. 15 Kernel density estimates (KDE) plots of magmatic and inherited zircon ages of Aserradero Rhyolite and selected Palaeozoic acidic rocks of Mexico and Guatemala. **a** Aserradero Rhyolite, this work. **b** Maxala (Martínez-Sánchez 2016). **c** Altos Cuchumatanes, Guatemala (Solari et al. (2010b). **d** Totoltepec Pluton (Kirsch et al. 2012). **e** Yucatán granitoids (Zhao et al. 2020). **f** Western Gulf of Mexico granitoids (Coombs et al. 2019). **g** Cuanana Pluton and Honduras Batolith (Ortega-Obregón et al. 2014). **h** Las Delicias Arc (Lopez 1997), granite cobbles in Tecomate Fm (Keppie et al. 2004), and La Carbonera Stock (Solari et al. 2001). The defined bin width is 50 Ma. The KDE plots were generated with the software IsoplotR (Ludwig 2012)

(1965). The similarity of these Pennsylvanian ages may indicate a correlation between the cooling phase of the Peregrina Tonalite and the Granjeno–Acatlán metamorphism. It is plausible to assume that the cooling ages correspond to cooling after reheating during the final latest Carboniferous collision (Ouachita Orogeny). It is therefore also plausible to assume that the Ordovician tonalite was exposed during the eruption of the Aserradero Rhyolite. Ordovician detrital zircons in quartzites of the Granjeno Complex indicate that the tonalite was outcropping at least since Devonian times, corresponding to the maximal deposition age of the metamorphosed protoliths (Barboza-Gudiño et al. 2011). On the other hand, the Aserradero Rhyolite shows no evidence of having been influenced by the Late Pennsylvanian orogenic event (300 ± 4 Ma, Dowe et al. 2005; Torres-Sánchez et al. 2016).

Geotectonic interpretation

It is remarkable that after a profuse Ordovician magmatic activity along the northwestern margin of Gondwana, a period of magmatic paucity followed during the entire Devonian and the early Carboniferous. It is not until the Early Mississippian when the magmatic activity resumed in a region bordering the northwestern margin Gondwana, namely with the Aserradero Rhyolite. This magmatic activity continued until Permian times, accompanying the closure of the Rheic Ocean when the southern edge of the Laurentia plate was subducted beneath the Gondwanan continental-margin arc. The collisional Ouachita-Marathon-Sonora orogenic belt began in mid-Mississippian time and ended diachronously in the Late Pennsylvanian in the Ouachita Mountains, Early Permian in the Marathon region, and Late Permian in Sonora (Poole et al. 2005).

It is important to note that paradigmatic interpretations for the origin of the Carboniferous–Permian arc have evolved, from the predomination of circum-Atlantic collisions to accretionary tectonics of circum-Pacific terranes and subduction, finally to a southward subduction related to the termination of the Rheic Ocean.

Woods et al. (1991) postulated in their detailed compilation from subsurface pre-Triassic granitoids sampled by several oil exploration wells in Mexico (NE and E-central Mexico, Coahuila, Nuevo Leon and Tamaulipas) that a huge granitic batholith (Fig. 1) underlies a Late Palaeozoic island-arc system that collided with the eastern continental Atlantic margin of Mexico. Torres et al. (1999) proposed that the NW–SE-oriented belt of Permo–Triassic arc granitoids in Mexico was related to the east-dipping subduction along the western margin of Pangaea. Several authors explained a number of Carboniferous-Permian arc granitoids along with Mexico and Central America by this model (e.g., Solari et al. 2001, 2010b; Keppie et al. 2004; Kirsch et al. 2012; Ortega-Obregón et al. 2014). The ~ 326 Ma adakitic Yucatán granitoids of the Maya Block (Zhao et al. 2020) were interpreted in terms of crustal anatexis caused by asthenospheric upwelling resulting from slab-breakoff, and not within a continental arc setting.

Recently, Coombs et al. (2019) defined three magmatic phases in the western Gulf of Mexico, related to the Pangaea amalgamation, all of which clearly younger than Aserradero Rhyolite. The first phase corresponds to a continental arc tectonic setting, before the final assembling of Pangea during the Early Permian (294–274 Ma). This phase could be considered analogous to the Late Carboniferous–Early Permian granitoids that intrude the Acatlán and Oaxacan complexes. The second phase, during the Late Permian–Early Triassic (263–243 Ma), is interpreted in terms of late- to postcollisional magmatism following the assembly of Pangea. Finally, the third phase, a synchronous supra-subduction magmatism, is associated with the Nazas arc system during the Early–Middle Jurassic (189–164 Ma).

From comparison to other Palaeozoic magmatic complexes, we interpret the Early Mississippian Aserradero Rhyolite to represent the first pre-collisional episode of the Carboniferous to Early Permian magmatic arc in Mexico. Members of this arc are included in the Acatlán Complex, the Oaxaca Block and the Maya Block, except the Aserradero Rhyolite which was erupted during the deposition of the Tamatán Group over the Novillo Complex (Fig. 16a). In our palaeogeographic interpretations, it is important to note that deposition of thick sedimentary Tamatán Group requires that the Ciudad Victoria sector of Oaxaquia must have been separated from continental Gondwana at the time of the deposition (Fig. 16a). This further implies that Oaxaquia acted as a peri-Gondwanan crustal block, which slowly approached Laurentia during the Late Carboniferous. The southward subduction of the oceanic plate under Oaxaquia (Fig. 16b) accompanied the diachronic closure of the Rheic Ocean as well as the generation of magmas with continental arc geochemical signatures. During the Ouachita-Marathon-Sonora Orogeny, the Oaxaquia peri-Gondwanan crustal block was trapped between Gondwana and Laurentia. Later, probably during the latest Permian and/or the Early Triassic, the Late Pennsylvanian Granjeno Complex overthrusted the Novillo Complex, together with the Peregrina Tonalite and the Tamatán Group.

No evidence other than the Aserradero Rhyolite indicating Early Mississippian subduction has been reported for northeastern Mexico. On the other hand, Estrada-Carmona et al. (2016) dated garnets from eclogites of the Piaxtla Suite and the Asís Lithodeme in the Acatlán Complex by the Lu–Hf method at 352.5 ± 1.6 Ma, which implies active subduction during this time. Similar ages of both units, the Aserradero Rhyolite as well as the Piaxta and Asís eclogites, suggest a similar tectonic setting during the

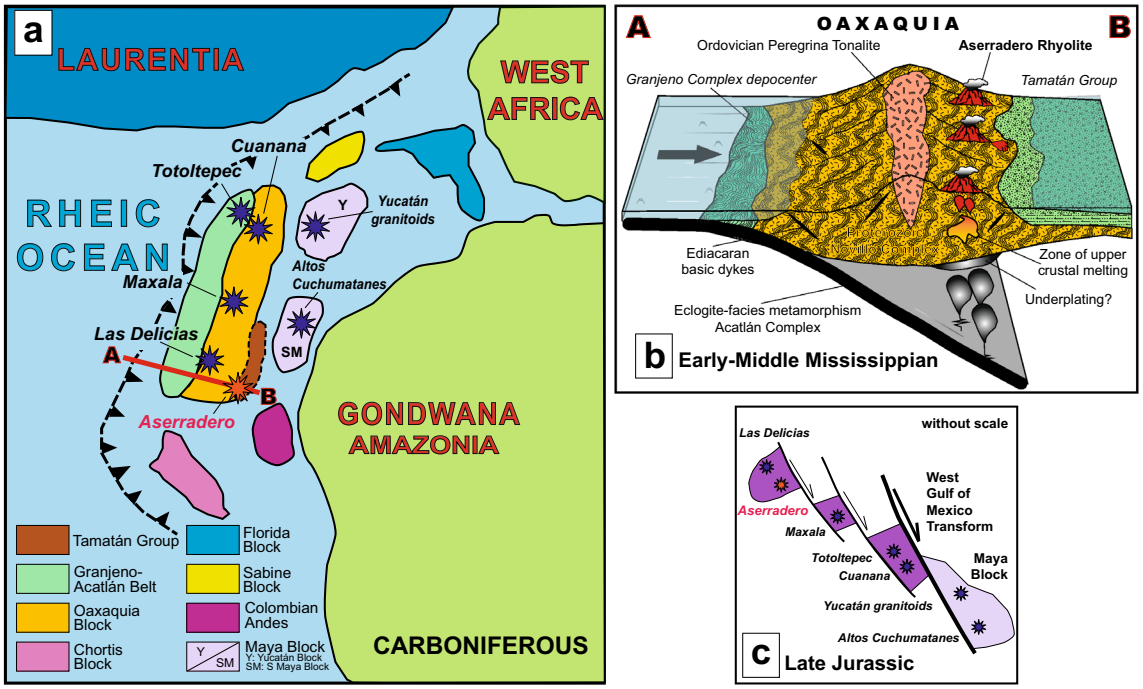

Fig. 16 **a** Palaeogeographic setting during the Carboniferous for the peri-Gondwanan terranes. Modified after Weber et al. (2007), Ortega-Obregón et al. (2014), and Zhao et al. (2020). The stars represent the compared localities of Carboniferous to Early Permian arc rocks mentioned in the text. **b** A–B schematic block diagram indicated in **a**, representing the proposed model for the position of the Aserradero Rhyolite volcanism during the Early to Middle Mississippian on the margin of the Tamatán Basin, in agreement with Alemán-Gallardo et al. (2019a), before the Late Pennsylvanian metamorphism and the Late Permian to Early Triassic tectonic emplacement of the Granjeno Complex over the Novillo Complex and the Tamatán Group. Eclogite-facies metamorphism (352.5 Ma) in the Acatlán Complex from Estrada-Carmona et al. (2016). **c** Phases of shearing and migration of the crustal blocks of Mexico, during the Late Jurassic opening of the Gulf of Mexico, modified after Coombs et al. (2019)

Carboniferous (Fig. 16b). The Santa Rosa Formation in the Chiapas State, consisting mainly of slates, phyillites, and sandstones, contains a cluster of youngest Mississippian detrital zircon grains ranging in age from 341 to 331 Ma, indicating the maximum age of deposition (Weber et al. 2009). These ages are indistinguishable from those of the Aserradero Rhyolite eruptions. Hence, it is plausible to suggest that these zircon grains deposited coeval with the rhyolitic eruption in close vicinity (Fig. 16a).

The Oaxaquia crustal block was, according to our interpretations and in agreement with Coombs et al. (2019), oriented SW–NE before the closure of the Rheic Ocean. It is during the Upper Jurassic opening of the Gulf of Mexico when this block as well as the Maya block (composed by the Yucatán and the Southern Maya Block; e.g. Pindell et al. 2005) were dissected and drifted southwards along strike-slip faults (Fig. 16c). Considering this hypothesis, the region of Ciudad Victoria remained closer to the collision zone, in a more autochthonous position than the Chiapas and Oaxacan Complexes. This configuration allows the development and preservation of the NW–SE alignment of the basement units of the core of the HPA, without the need for a large rotation (Fig. 2b).

Some decades ago, several authors applied the concept of tectonostratigraphic terranes to the group and to correlate the different basement units exposed near Ciudad Victoria and the surrounding areas. Campa and Coney (1983) coined the concept to the '*Sierra Madre Terrane*' for the Precambrian metamorphic basement and the covering Palaeozoic and Mesozoic sedimentary rocks in the north-central part of Mexico. This definition changed later, as expressed by Sedlock et al. (1993), with the introduction of the '*Guachichil Terrane*' to include the whole basement in the core of the Huizachal–Peregrina and Huayacocotla anticlines. The latter terrane comprises the complete Triassic-Cretaceous stratigraphic sequence of the Sierra Madre Oriental, too. Later, Keppie (2004) suggested that the Sierra Madre Terrane should be restricted to the Granjeno Complex, excluding the Novillo Complex. In a contrasting vision, Ortega-Gutiérrez et al. (2018) considered that the terranes of the Huastecan orogenic belt (including the Granjeno Complex) define a NNW–SSE oriented suture

belt separating the Grenvillian terranes to the west from the late Neoproterozoic of the northern Maya to the east.

To date, there is no clear consensus about the definition or even the existence of these terranes and is the reason why we prefer to abandon their use. Instead, and considering that the basement units exposed near Ciudad Victoria and in Nuevo León are correlative to exposures from other Mexican regions, we suggest the concept of the '*Ciudad Victoria Block*'. This block (consisting of Novillo Complex, Peregrina Tonalite, Granjeno Complex and Tamatán Group) was separated from the other segments of Oaxaquia and their attached units during the Upper-Jurassic Gulf of Mexico opening.

Conclusions

In this study, we present the first interpretation of the Early to Middle Mississippian Aserradero Rhyolite, a unique volcanic unit contained in the Palaeozoic Tamatán Group of the Sierra Madre Oriental basement in NE Mexico.

The crystallisation age of the studied rhyolites is now well constrained to 347.8 ± 2.7 Ma and 340.7 ± 3.6 Ma using U–Pb LA-ICP-MS analysis of zircons. The Aserradero Rhyolite has geochemical features equivalent to high-K, low-Sr, and S-type granitoids, probably produced by an upper-crustal source similar to that of the Novillo Complex.

These subaerial rhyolitic flows postdate an exhumation and deformational period of the underlying pre-Early Mississippian units (the Proterozoic Novillo Complex, the Ordovician Peregrina Tonalite, and the lower part of the Tamatán Group) of the NE Mexican basement. This exhumation process and the subsequent eruption of the rhyolitic lavas occurred before the greenschist metamorphism of the Granjeno Complex and its later emplacement above the continental crust, probably during late Permian times along the 'Don Eliborio Manzano' thrust fault. The palaegeographic reconstructions for Carboniferous times indicate that Oaxaquia was not attached to Gondwana, because the depocenter where the Tamatán Group was deposited needs to be accommodated between them.

Based on the correlation to other Carboniferous–Early Permian magmatic complexes in Mexico, we suggest that the Aserradero Rhyolite represents an early, pre-collisional stage of the peri-Gondwanan Carboniferous–Permian magmatic arc, present also in Las Delicias, Oaxaquia, the Acatlán Complex, the Maya Block, as well as in the crystalline basement along the Western Gulf of Mexico.

We propose the concept of a '*Ciudad Victoria Block*' for the assembly of Novillo Complex, Peregrina Tonalite, Granjeno Complex and Tamatán Group. We suggest that this block was dismembered from Oaxaquia and their peripheral units during the Upper-Jurassic Gulf of Mexico opening.

Acknowledgements We wish to thank C. Ortega-Obregón and L. Solari for the assistance during the analytical procedures. We also thank Don Eliborio Manzano, a modest farmer and field guide in the deepest parts of the Peregrina Canyon, for allowing us to stay on his land and for useful fieldwork tips. We are also very grateful to V. Leal-Cuéllar for the support provided in the field campaigns. Co-authors Alemán-Gallardo and Casas-Peña thank the Consejo Nacional de Ciencia y Tecnología (CONACyT, Mexico) for financial support during their MSc and PhD programs at the Universidad Autónoma de Nuevo León, Facultad de Ciencias de la Tierra, Mexico. The first author expresses his gratitude to the German Academic Exchange Service for the support provided to participate in the Latin-American Colloquium of Geosciences 2019 at the Institute of Geology, Universität Hamburg. This paper benefited significantly from very constructive and critical suggestions from U. Riller, B. Weber, and M. Kirsch. Additionally, we thank L. Waite for his grammar suggestions to improve this work.

References

Alemán-Gallardo EA, Ramírez-Fernández JA, Rodríguez-Díaz AA, Velasco-Tapia F, Jenchen U, Cruz-Gámez EM, De León-Barragán L, Navarro-De León I (2019a) Evidence for an Ordovician continental arc in the pre-Mesozoic basement of the Huizachal-Peregrina Anticlinorium, Sierra Madre Oriental, Mexico: Peregrina Tonalite. Miner Petrol 113:505–525

Alemán-Gallardo EA, Ramírez-Fernández JA, Weber B, Velasco-Tapia F, Casas-Peña JM (2019b) Novillo Metamorphic Complex, Huizachal-Peregrina Anticlinorium, Tamaulipas, Mexico: characterization and development based on whole-rock geochemistry and Nd-isotopic ratios. J S Am Earth Sci 96:102382

Annen C, Blundy JD, Sparks RSJ (2006) The genesis of intermediate and silicic magmas in deep crustal hot zones. J Petrol 47:505–539

Barboza-Gudiño JR, Ramírez-Fernández JA, Torres-Sánchez SA, Valencia VA (2011) Geocronología de circones detríticos de diferentes localidades del Esquisto Granjeno en el noreste de México. Bol Soc Geol Mex 63:201–216

Boucot AJ, Blodgett R, Stewart JH (1997) European province late Silurian brachiopods from the Ciudad Victoria area, Tamaulipas, northeastern Mexico. Geol Soc Am Special Paper 321:273–294

Cameron KL, Lopez R, Ortega-Gutiérrez F, Solari LA, Keppie JD, Schulze C (2004) U-Pb geochronology and Pb isotopic compositions of leached feldspars: Constraints on the origin and evolution of Grenville rocks from Eastern and southern Mexico. Geol Soc Am Memoir 197:755–769

Campa MF, Coney PJ (1983) Tectono-stratigraphic terranes and mineral resource distributions in Mexico. Can J Earth Sci 20:1040–1051

Cardona A, Valencia VA, Lotero A, Villafañez Y, Bayona G (2016) Provenance of middle to late Palaeozoic sediments in the northeastern Colombian Andes: implications for Pangea reconstruction. Int Geol Rev 58:1914–1939

Carrillo-Bravo J (1961) Geología del Anticlinorio Huizachal-Peregrina al NE de Cd. Victoria. Tamaulipas Bol Asoc Mex Geól Petrol 13:1–98

Casas-García R (2014) Caracterización petrológica de las nelsonitas precámbricas del complejo Gneis Novillo, NE de México. MSc thesis, Universidad Autónoma de Nuevo León, México

Castillo–Rodríguez H (1988) Zur Geologie des kristallinen Grundgebirges der Sierra Madre Oriental – insbesondere des Granjeno–Schiefer Komplexes im Südteil

des Huizachal–Peregrina–Antiklinoriums (Raum Ciudad Victoria, Tamaulipas, Mexiko). MSc thesis, Westfälische Wilhelms-Universität in Münster, Germany

Catuneanu O (2004) Retroarc foreland systems—evolution through time. J Afr Earth Sci 38:225–242

Centeno-García E, Mendoza CC, Silva-Romo G (2009) Sedimentología de la Formación Matzitzi (Paleozoico superior) y significado de sus componentes volcánicos, región de Los Reyes Metzontla-San Luis Atolotitlán, Estado de Puebla. Rev Mex Ciencias Geol 26:18–36

Chappell B, White A (1974) Two contrasting granite types. Pac Geol 8:173–174

Coombs H, Kerr A, Pindell J, Buchs D, Weber B, Solari L (2019) Petrogenesis of the crystalline basement along the western Gulf of Mexico: Postcollisional magmatism during the formation of Pangea. Southern and central Mexico: basement framework, tectonic evolution, and provenance of Mesozoic-Cenozoic basins. Geol Soc Am Special Paper. https://doi.org/10.1130/2020.2546(02)

De León-Barragán L, Ramírez-Fernández JA (2012) Magmatismo de Arco del Carbonífero de la margen NW de Gondwana en el Estado de Tamaulipas, México. Simposio Geología de la Sutura Laurencia Gondwana en Chihuahua, October 2012. Universidad Autónoma de Chihuahua, Chihuahua, pp 56–58

Dowe DS, Nance RD, Keppie JD, Cameron KL, Ortega-Rivera A, Ortega-Gutierrez F, Lee JWK (2005) Deformational history of the Granjeno Schist, Ciudad Victoria, Mexico: constraints on the closure of the Rheic Ocean? Int Geol Rev 47:920–937

Drüppel K, McCready AJ, Stumpfl EF (2009) High-K granites of the Rum Jungle Complex, N-Australia: insights into the Late Archean crustal evolution of the North Australian Craton. Lithos 111(3–4):203–219

Ducea MN, Paterson SR, DeCelles PG (2015) High-volume magmatic events in subduction systems. Elements 11:99–104

Elías-Herrera M, Ortega-Gutiérrez F (2002) Caltepec fault zone: an Early Permian dextral transpressional boundary between the Proterozoic Oaxacan and Paleozoic Acatlán complexes, southern Mexico, and regional tectonic implications. Tectonics 21:1–18

Elías-Herrera M, Ortega-Gutiérrez F, Sánchez-Zavala JL, Macías-Romo C, Ortega-Rivera A, Iriondo A (2005) La falla de Caltepec: raíces expuestas de una frontera tectónica de larga vida entre dos terrenos continentales del sur de México. Bol Soc Geol Mex 57:83–109

Esquivel-Macías C, Solís-Marín FY, Buitrón-Sánchez BE (2004) New records of Upper Paleozoic crinoids columnar plates (Echinodermata, Crinoidea) from Upper Paleozoic of Mexico, some paleobiogeographic and paleoenvironmental implications. Coloquios de Paleontología 54:15–23

Estrada-Carmona J, Weber B, Martens U, López-Martínez M (2012) Petrogenesis of Ordovician magmatic rocks in the southern Chiapas Massif Complex: relations with the early Palaeozoic magmatic belts of northwestern Gondwana. Int Geol Rev 54:1918–1943

Estrada-Carmona J, Weber B, Scherer EE, Martens U, Elías-Herrera M (2016) Lu-Hf geochronology of Mississippian high-pressure metamorphism in the Acatlán Complex, southern México. Gondwana Res 34:174–186

Fitz-Díaz E, Lawton TF, Juárez-Arriaga E, Chávez-Cabello G (2018) The Cretaceous-Paleogene Mexican orogen: Structure, basin development, magmatism, and tectonics. Earth Sci Rev 183:56–84

Flores de Dios Gonzalez LA, Vachard D, Buitrón Sanchez BE (1998) The Tiñu, Santiago Ixtaltepec and Yododene Formations, Oaxaca State: sedimentological, stratigraphic and paleogeographic reinterpretations. In: Program IGC (ed) Laurentia-Gondwanan Connections before Pangea. Program and Abstracts. Instituto de Geología-Universidad Nacional Autónoma de Mexico, Oaxaca, p 16

Fries C Jr, Rincón-Orta C (1965) Nuevas aportaciones geocronológicas y técnicas empleadas en el Laboratorio de Geocronometría. Bol Inst Geol UNAM 73:57–133

Frost BR, Barnes CG, Collins WJ, Arculus RJ, Ellis DJ, Frost CD (2001) A geochemical classification for granitic rocks. J Petrol 42:2033–2048

Gillis RJ, Gehrels GE, Ruiz J, Flores de Dios-González LA (2005) Detrital zircon provenance of Cambrian-Ordovician and Carboniferous strata of the Oaxaca terrane, southern Mexico. Sediment Geol 182:87–100

Gómez JC (2014) Braquiópodos del Ordovícico Medio y Silúrico del flanco surandino: Venezuela. Geominas 42:13–18

González-Guzmán R, Weber B, Manjarrez-Juárez R, Cisneros de León A, Hecht L, Herguera-García JC (2016) Provenance, age constraints and metamorphism of Ediacaran metasedimentary rocks from the El Triunfo Complex (SE Chiapas, México): evidence for Rodinia breakup and Iapetus active margin. Int Geol Rev 58:2065–2091

Grimes CB, Wooden JL, Cheadle MJ, John BE (2015) "Fingerprinting" tectono-magmatic provenance using trace elements in igneous zircon. Contrib Mineral Petrol 170:1–26

Gursky HJ (1996) Palaeozoic stratigraphy of the Peregrina Canyon area, Sierra Madre Oriental. Zbl Geol Paläont Teil I Heft 7(8):973–989

Gursky H-J, Michalzik D (1989) Lower Permian turbidites in the northern Sierra Madre Oriental. Mexico: Zbl Geol Pal. Teil I:821–838

Gursky H-J, Ramírez-Ramírez C (1986) Notas preliminares sobre el descubrimiento de volcanitas ácidas en el Cañón de Caballeros (Núcleo del Anticlinorio Huizachal-Peregrina, Tamaulipas, México). Actas Fac Ciencias Tierra UANL 1:11–22

Gutiérrez-Marco JC, Goldman D, Reyes-Abril J, Gómez J (2011) A preliminary study of some Sandbian (Upper Ordovician) graptolites from Venezuela. In: Gutiérrez-Marco JC, Rábano I, García-Bellido D (eds) Ordovician of the world, vol 14. Instituto Geológico y Minero de España, Cuadernos del Museo Geominero, Madrid, pp 199–206

Hoskin PW, Schaltegger U (2003) The composition of zircon and igneous and metamorphic petrogenesis. Rev Mineral Geochem 53:27–62

Ibañez-Mejia M, Bloch EM, Vervoort JD (2018) Timescales of collisional metamorphism from Sm-Nd, Lu-Hf and U-Pb thermochronology: a case from the Proterozoic Putumayo Orogen of Amazonia. Geochim Cosmochim Ac 235:103–126

Keppie JD (2004) Terranes of Mexico revisited: A 1.3 billion year Odyssey. Int Geol Rev 46:765–794

Keppie JD, Sandberg ChA, Miller BV, Sánchez-Zavala JL, Nance RD, Poole FG (2004) Implications of Latest Pennsylvanian to Middle Permian Paleontological and U-Pb SHRIMP Data from the Tecomate Formation to Re-dating Tectonothermal Events in the Acatlán Complex, Southern Mexico. Int Geol Rev 46:745–753

Kirsch M, Keppie JD, Murphy JB, Solari LA (2012) Permian-Carboniferous arc magmatism and basin evolution along the western margin of Pangea: geochemical and geochronological evidence from the eastern Acatlán Complex, southern Mexico. Geol Soc Am Bull 124:1607–1628

Lawlor PJ, Ortega-Gutiérrez F, Cameron KL, Ochoa-Camarillo H, Lopez R, Sampson DE (1999) U-Pb geochronology, geochemistry, and provenance of the Grenvillian Huiznopala Gneiss of Eastern Mexico. Precambrian Res 94:73–99

Laya JC, Tucker ME (2012) Facies analysis and depositional environments of Permian carbonates of the Venezuelan Andes: Palaeogeographic implications for Northern Gondwana. . Palaeogeogr Palaeoclimatol Palaeoecol 331–332:1–26

Le Bas MJ, Le Maitre RW, Streckeisen A, Zanettin B (1986) A chemical classification of volcanic rocks based on the total alkali-silica diagram. J Petrol 27:745–750

Le Maitre RW, Bateman P, Dudek A, Keller J, Lameyre J, Le Bas MJ, Sabine R, Schmid R, Sørensen A, Steckeisen A, Woolley AR, Zanettin B (1989) A classification of igneous rocks and glossary of terms. Recommendations of the IUGS Subcommission on the Systematics of Igneous rocks. Blackwell Scientific Publications, London

Lee C-TA, Morton DM, Kistler RW, Baird AK (2007) Petrology and tectonics of Phanerozoic continent formation: from island arcs to accretion and continental arc magmatism. Earth Planet Sci Lett 263:370–387

Lopez R (1997) High-Mg Andesites Form the Gila Bend Mountains, Southwestern Arizona, Evidence for Hydrous Melting of Lithosphere During Miocene Extension and The Pre-jurassic Geotectonic Evolution of the Coahuila Terrane, Northwestern Mexico, Grenville Basement, a Late Paleozoic Arc, Triassic Plutonism, and the Events South of the Ouachita Suture. PhD thesis University of California, Santa Cruz

Ludwig KR (2012) Isoplot/Ex, v. 3.75. Berkeley Geochronology Center Special Publication, 5

Martens U, Weber B, Valencia VA (2010) U/Pb geochronology of Devonian and older Paleozoic beds in the southeastern Maya block, Central America: its affinity with peri-Gondwanan terranes. Geol Soc Am Bull 122:815–829

Martínez-Sánchez LE (2016) Estudio Geológico, Geoquímico y Geocronológico del Granito Maxala, del magmatismo Carbonífero de México (Hidalgo y Veracruz). BSc thesis Instituto Politécnico Nacional, Mexico

McDonough WF, Sun SS (1995) The composition of the Earth. Chem Geol 120:223–253

McKee JW, Jones NW, Anderson TH (1999) The Late Paleozoic and Early Mesozoic history of the Las Delicias terrane, Coahuila, Mexico. - in: Bartolini, C., Wilson, J.L., Lawton, T.F. (eds.): Mesozoic sedimentary and tectonic history of north-central Mexico. Geol Soc Am Special Paper 340:161–189

Middlemost EA (1989) Iron oxidation ratios, norms, and the classification of volcanic rocks. Chem Geol 77:19–26

Murphy JB, Pisarevsky SA, Nance RD, Keppie JD (2004) Neoproterozoic-Early Paleozoic evolution of peri-Gondwanan terranes: implications for Laurentia-Gondwana connections. Int J Earth Sci 93:659–682

Navarro-Santillan D, Sour-Tovar F, Centeno-Garcia E (2002) Lower Mississippian (Osagean) brachiopods from the Santiago Formation, Oaxaca, Mexico: stratigraphic and tectonic implications. J S Am Earth Sci 15:327–336

Orozco-Esquivel MT (1990) Zur Petrologie des Kristallins im Huizachal-Peregrina-Fenster. Sierra Madre Oriental, Mexiko. MSc thesis, Universität Karlsruhe, Germany

Ortega-Gutiérrez F, Ruiz J, Centeno-García E (1995) Oaxaquia, a Proterozoic microcontinent accreted to North America during the late Paleozoic. Geology 23:1127–1130

Ortega-Gutiérrez F, Elías-Herrera M, Morán-Zenteno DJ, Solari L, Weber B, Luna-González L (2018) The pre-Mesozoic metamorphic basement of Mexico, 1.5 billion years of crustal evolution. Earth Sci Rev 183:2–37

Ortega-Obregón C, Solari LA, Keppie JD, Ortega-Gutiérrez F, Solé J, Morán-Ical S (2008) Middle-Late Ordovician magmatism and Late Cretaceous collision in the southern Maya block, Rabinal-Salamá area, central Guatemala: implications for North America-Caribbean plate tectonics. Geol Soc Am Bull 120:556–570

Ortega-Obregón C, Solari L, Gómez-Tuena A, Elías-Herrera M, Ortega-Gutiérrez F, Macías-Romo C (2014) Permian-Carboniferous arc magmatism in southern Mexico: U-Pb dating, trace element and Hf isotopic evidence on zircons of earliest subduction beneath the western margin of Gondwana. Int J Earth Sci 103:1287–1300

Paton C, Woodhead JD, Hellstrom JC, Hergt JM, Greig A, Maas R (2010) Improved laser ablation U-Pb zircon geochronology through robust downhole fractionation correction. Geochem Geophys Geosyst 11:3

Paton C, Hellstrom J, Paul B, Woodhead J, Hergt J (2011) Iolite: Freeware for the visualization and processing of mass spectrometric data. J Anal Atom Spectrom 26:2508

Pearce JA, Peate DW (1995) Tectonic implications of the composition of volcanic arc magmas. Annu Rev Earth Planet Sci 23:251–285

Pearce JA, Harris NB, Tindle AG (1984) Trace element discrimination diagrams for the tectonic interpretation of granitic rocks. J Petrol 25:956–983

Peccerillo A, Taylor R (1976) Geochemistry of Eocene calc-alkaline volcanic rocks from the Alban Hills (Roman comagmatic region) as inferred from trace element geochemistry. Contrib Mineral Petrol 58:63–81

Petrus JA, Kamber BS (2012) VizualAge: a novel approach to laser ablation ICP-MS U-Pb geochronology data reduction. Geostand Geoanal Res 36:247–270

Pindell J, Kennan L, Maresch WV, Stanek KP, Draper G, Higgs R (2005) Plate-kinematics and crustal dynamics of circum-Caribbean arc-continent interactions: Tectonic controls on basin development in Proto-Caribbean margins, in Avé Lallemant HG Sisson VB, eds, Caribbean-South American plate interactions, Venezuela. Geol Soc Am Special Paper 394:7–52

Poole FG, Perry WJ, Madrid RJ, Amaya-Martínez R (2005) Tectonic synthesis of the Ouachita-Marathon-Sonora orogenic margin of southern Laurentia: Stratigraphic and structural implications for timing of deformational events and plate-tectonic model. Geol Soc Am Special Paper 393:543–596

Ramírez-Fernández JA, Jenchen U (2016) Cinturones orogénicos sepultados bajo la Sierra Madre Oriental: basamento precámbrico y paleozoico. Ciencia UANL 19:47–53

Ramírez-Ramírez C (1992) Pre-Mesozoic geology of Huizachal-Peregrina Anticlinorium, Ciudad Victoria, Tamaulipas, and adjacent parts of eastern Mexico. PhD thesis, The University of Texas at Austin, USA

Rosales-Lagarde L, Centeno-García E, Dostal J, Sour-Tovar F, Ochoa-Camarillo H, Quiroz-Barroso S (2005) The Tuzancoa Formation: evidence of an Early Permian Submarine Continental Arc in East-Central Mexico. Int Geol Rev 47:901–919

Rubatto D (2017) Zircon: the metamorphic mineral. Rev Mineral Geochem 83:261–295

Sánchez-Zavala JL, Ortega-Gutiérrez F, Keppie JD, Jenner JA, Belousova E, Macías-Romo C (2004) Ordovician and Mesoproterozoic Zircons from the Tecomate Formation and Esperanza Granitoids, Acatlán Complex, Southern Mexico: local Provenance in the Acatlán and Oaxacan Complexes. Int Geol Rev 46:1005–1021

Schulze-Schreiber CH (2011) Petrología y geoquímica de las rocas de Pluma Hidalgo, Oaxaca e implicaciones tectónicas para el Proterozoico de "Oaxaquia". PhD thesis, Instituto de Geología, Universidad Nacional Autónoma de México, Mexico

Sedlock RL, Ortega-Gutiérrez F, Speed RC (1993) Tectonostratigraphic terranes and tectonic evolution of Mexico: Boulder, Colorado. Geol Soc Am Special Paper, Colorado, p 278

Slama J, Košler J, Condon DJ, Crowley JL, Gerdes A, Hanchar JM, Horstwood MSA, Morris GA, Nasdala L, Norberg N, Schaltegger U, Schoene B, Tubrett MN, Whitehouse MJ (2008) Plešovice zircon—a new natural reference material for U-Pb and Hf isotopic microanalysis. Chem Geol 249:1–35

Solari LA, Dostal J, Gutiérrez FO, Keppie JD (2001) The 275 Ma arc-related La Carbonera stock in the northern Oaxacan Complex of

southern Mexico: U-Pb geochronology and geochemistry. Rev Mex Cienc Geol 1:149–161
Solari LA, Keppie JD, López R, Cameron KL, Ortega-Gutiérrez F (2004) ~ 990 Ma peak granulitic metamorphism and amalgamation of Oaxaquia, Mexico: U-Pb zircon geochronological and common Pb isotopic data. Rev Mex Cienc Geol 21:212–225
Solari LA, Gómez-Tuena A, Bernal JP, Pérez-Arvizu O, Tanner M (2010a) U-Pb Zircon Geochronology with an Integrated LA-ICP-MS Microanalytical Workstation: achievements in precision and accuracy. Geostand Geoanal Res 34:5–18
Solari LA, Ortega-Gutiérrez F, Elías-Herrera M, Gómez-Tuena A, Schaaf P (2010b) Refining the age of magmatism in the Altos Cuchumatanes, western Guatemala, by LA–ICPMS, and tectonic implications. Int Geol Rev 52:977–998
Sour-Tovar F, Álvarez F, Martínez Chacón ML (2005) Lower Mississippian (Osagean) spire-bearing Brachiopods from Cañón de la Peregrina, North of Ciudad Victoria, Tamaulipas, northeastern México. J Paleontol 79:469–485
Stewart JH, Blodgett RB, Boucot AJ, Carter JL, Lopez R (1999) Exotic Paleozoic strata of Gondwanan provenance near Ciudad Victoria, Tamaulipas, Mexico, vol 336. In: Ramos VA, Keppie JD (eds) Laurentia-Gondwana connections before Pangea. Geol Soc Am Special Paper, Boulder, pp 227–252
Sun SS, McDonough WF (1989) Chemical and isotopic systematics of oceanic basalts: implications for mantle composition and processes. Geol Soc London Sp Pub 42:313–345
Tazzo-Rangel MD, Weber B, González-Guzmán R, Valencia VA, Frei D, Schaaf P, Solari LA (2018) Multiple metamorphic events in the Palaeozoic Mérida Andes basement, Venezuela: insights from U-Pb geochronology and Hf–Nd isotope systematics. Int Geol Rev. https://doi.org/10.1080/00206814.2018.1522520
Torres R, Ruiz J, Patchett PJ (1999) Permo-Triassic continental arc in Eastern Mexico: Tectonic implications for reconstructions of southern North America. Geol Soc Am Special Paper 340:191–196
Torres-Martínez MA, Sour-Tovar F (2016) Braquiópodos discínidos (Lingulida, Discinoidea) de la Formación Ixtaltepec, Carbonífero del área de Santiago Ixtaltepec, Oaxaca. Bol Soc Geol Mex 68:313–321
Torres-Sánchez SA, Augustsson C, Barboza-Gudiño JR, Jenchen U, Ramírez-Fernández JA, Abratis M, Scherstén A (2016) Magmatic source and metamorphic grade of metavolcanic rocks from the Granjeno Schist: was northeastern Mexico a part of Pangaea? Geol J 51:845–863
Torres-Sánchez SA, Augustsson C, Jenchen U, Barboza-Gudiño JR, Alemán-Gallardo EA, Ramírez-Fernández JA, Torres-Sánchez D, Abratis M (2017) Petrology and geochemistry of meta-ultramafic rocks in the Paleozoic Granjeno Schist, northeastern Mexico: Remnants of Pangaea ocean floor. Open Geosci 9:361–384
Trainor RJ (2010) Structural/Kinematic and Metamorphic Analysis of the Mesoproterozoic Novillo Gneiss, Tamaulipas, Mexico. MSc thesis, Ohio University, USA
Trainor RJ, Nance RD, Keppie JD (2011) Tectonothermal history of the Mesoproterozoic Novillo Gneiss of eastern Mexico: support for a coherent Oaxaquia microcontinent. Rev Mex Cienc Geol 28:580–592
Van der Lelij R, Spikings R, Ulianov A, Chiradia M, Mora A (2016) Paleozoic to Early Jurassic history of the northwestern corner of Gondwana, and implications for the evolution of the Iapetus, Rheic, and Pacific Oceans. Gondwana Res 31:271–294
Verma SP, Torres-Alvarado IS, Sotelo-Rodríguez ZT (2002) SINCLAS: standard igneous norm and volcanic rock classification system. Comput Geosci 28:711–715
Weber B, Schulze CH (2014) Early Mesoproterozoic (> 1.4 Ga) ages from granulite basement inliers of SE Mexico and their implications on the Oaxaquia concept-Evidence from U-Pb and Lu-Hf isotopes on zircon. Rev Mex Cienc Geol 31(3):377–394
Weber B, Schaaf P, Valencia VA, Iriondo A, Ortega-Gutiérrez F (2006) Provenance ages of late Paleozoic sandstones (Santa Rosa Formation) from the Maya block, SE Mexico. Implications on the tectonic evolution of western Pangea. Rev Mex Cienc Geol 23:262–276
Weber B, Iriondo A, Premo WR, Hecht L, Schaaf P (2007) New insights into the history and origin of the southern Maya block, SE México: U-Pb–SHRIMP zircon geochronology from metamorphic rocks of the Chiapas massif. Int J Earth Sci 96:253–269
Weber B, Valencia VA, Schaaf P, Ortega-Gutiérrez F (2009) Detrital zircon ages from the Lower Santa Rosa Formation, Chiapas: implications on regional Paleozoic stratigraphy. Rev Mex Cienc Geol 26:260–276
Weber B, Scherer EE, Schulze C, Valencia VA, Montecinos P, Mezger K, Ruiz J (2010) U-Pb and Lu-Hf isotope systematics of lower crust from central-southern Mexico—geodynamic significance of Oaxaquia in a Rodinia Realm. Precambrian Res 182:149–162
Weber B, González-Guzmán R, Manjarrez-Juárez R, de León AC, Martens U, Solari L, Hecht L, Valencia V (2018) Late Mesoproterozoic to Early Paleozoic history of metamorphic basement from the southeastern Chiapas Massif Complex, Mexico, and implications for the evolution of NW Gondwana. Lithos 300:177–199
Weber B, Schmitt AK, Cisneros A, de León R, González-Guzmán, (2019) Coeval early Ediacaran breakup of Amazonia, Baltica, and Laurentia: evidence from micro-baddeleyite dating of dykes from the Novillo Canyon, Mexico. Geophys Res Lett 46(4):2003–2011
Whitney DL, Evans BW (2010) Abbreviations for names of rock-forming minerals. Am Mineral 95:185–187
Wiedenbeck M, Allé P, Corfu F, Griffin WL, Meier M, Oberli F, Von Quadt A, Roddick JC, Spiegel W (1995) Three natural zircon standards for U-Th-Pb, Lu-Hf, trace element and REE analyses. Geostand Geoanal Res 19:1–23
Woods RD, Salvador A, Miles AE (1991) Pre-Triassic. In: Salvador A (ed) Origin and development of the Gulf of Mexico basin. The Geology of North America vol. J, The Gulf of Mexico Basin J. Geol Soc Am, Boulder, pp 109–129
Zhao J, Xiao L, Gulick SP, Morgan JV, Kring D, Fucugauchi JU et al (2020) Geochemistry, geochronology and petrogenesis of Maya Block granitoids and dikes from the Chicxulub Impact Crater, Gulf of México: Implications for the assembly of Pangea. Gondwana Res 82:128–150
Zhou Y, Murphy MA, Hamade A (2006) Structural development of the Peregrina-Huizachal anticlinorium, Mexico. J Struct Geol 28:494–507